High-magnetic-field magnetization and magnetoresistance of a transition-metal-base spin glass: Zr-Mn†

H. C. Jones, A. G. Montgomery, and I. B. Lin
Indiana University, Bloomington, Indiana 47401

J. W. Lue
Oak Ridge National Laboratory, Oak Ridge, Tennessee 37830

H. Nadler
Rockwell Science Center, Thousand Oaks, California 91360

R. R. Hake*
University of California, Los Angeles, California 90024
(Received 18 February 1977)

The magnetization M and electrical resistivity ρ have been measured at $0 \leq H \leq 135$ kG and $1.2 \leq T \leq 27$ K for the transition metal hcp Zr containing Mn at concentrations $520 \leq c \leq 3100$ ppm. The primary results are (a) the measurements confirm earlier indications that Mn displays a localized magnetic moment when in solution in hcp Zr and suggest a Kondo temperature $T_K < 1.0$ K; (b) both the high-H saturation magnetization and the low-H susceptibility show that the spin S associated with Mn in Zr is 2.0 ± 0.2; (c) the impurity magnetization $\Delta M \equiv M(\text{alloy}) - M(\text{Zr})$ obeys the Blandin-Souletie-Tournier scaling $\Delta M/c = F(H/c, T/c)$, suggesting the dominance of a long-range oscillating Ruderman-Kittel-Kasuya-Yosida (RKKY)-like moment-moment interaction, as appears to exist in the more widely investigated non-transition-metal–host spin glasses; (d) the behavior of the resistivity, susceptibility, and reversible magnetization indicates that spin-freezing temperatures $T_0(c)$ (if such exist in Zr-Mn) are below the present 1.2-K temperature limit; (e) the high $T > T_0$, high $H \gg k_B T/g\mu_B$, Larkin-Khmel'nitskii (LK) prediction $\Delta M(\text{LK}) = \Delta M_s(1 - H_0/H)$ (ΔM_s is the impurity saturation magnetization, $H_0 \propto cV_0$, V_0 is the RKKY coefficient) does not account for the (i) T-dependence of ΔM, (ii) relatively low fields $40 \lesssim H_s \lesssim 130$ kG (at $520 \leq c \leq 3100$-ppm Mn) required for saturation of the impurity magnetization at 1.2 K; (f) fits of the measured $\Delta M(H)$ to the theoretical $\Delta M(\text{LK})$ at $H < H_s$, $c \geq 1690$-ppm Mn, yield $V_0 = 2.7 \times 10^{-37}$ erg cm^3 and hence an exchange parameter $|J_{\text{RKKY}}| \approx 0.5$ eV; (g) at $c = 520$-ppm Mn, $\Delta M(H)$ is close to the free-spin Brillouin magnetization and $\rho(H, T)$ can be fit to single-impurity theory: (i) $\Delta\rho(T, H = 0) \equiv \rho(\text{alloy}) - \rho(\text{Zr})$ to the Hamann-Fischer formula with $T_K \leq 1.0$ K, (ii) the spin-component magnetoresistance $\delta\rho_s(H > H_s)$ to the Béal-Monod and Weiner third-order perturbation formula with an exchange parameter $J_m = -0.2$ eV. In general, the present work indicates that localized-magnetic-moment (S, T_K, J_m) and high-$T > T_0$ spin-glass (BST scaling, V_0, J_{RKKY}) behavior of Mn in the transition-metal hcp Zr is rather similar to that of Mn in the noble metals. However, the present observations of relatively low fields H_s required for saturation of the impurity magnetization suggest cutoffs on the order of $H_s(c)$ in the internal molecular-field distribution and do not appear to agree with current $T > T_0$ theory. It is unclear whether the disagreement is a general property of metallic spin glasses, or is peculiar to transition-metal host systems or to alloys (such as the present) with relatively short electron mean free paths which might cause some damping of the RKKY oscillations.

I. INTRODUCTION

Several groups[1-7] have recently reported the results of high-magnetic-field magnetization studies on non-transition-metal hosts such as Cu, Ag, Au, and Zn, containing dilute additions of magnetic impurities at concentrations and temperatures where the magnetization is influenced by interactions between well-defined magnetic moments localized on the impurities. For such "spin glasses,"[8,9] the observed isothermal impurity magnetization $\Delta M \equiv M(\text{alloy}) - M(\text{host})$, as a function of applied magnetic field H, usually falls well below the free-spin Brillouin-function magnetization with nonsaturation even up to experimental $(H/T)_{\max}$ limits of about 60 kG K^{-1}.[5,10] However, it has been found[1-5] that $\Delta M(H, T)$ is in at least approximate accord with theoretical predictions[11-13] based on the indirect interaction of localized magnetic moments through the conduction electrons by means of the s-d Ruderman-Kittel-Kasuya-Yosida (RKKY) potential.[14,15] Furthermore, the observed $\Delta M(H, T)$ generally scales approximately[1-4,7,16] with concentration c as

$$\Delta M/c = F(T/c, H/c), \tag{1}$$

where, for a given alloy system, F is a function whose form does not depend upon c. Blandin,[17]

Souletie, and Tournier[18] (BST) have shown that Eq. (1) follows rather directly from a random-molecular-field H_m model[9,19] which assumes a long-range oscillating RKKY moment-moment interaction potential $V_R \propto r^{-3}$. "BST scaling" contrasts sharply with the expected scaling

$$\Delta M/c = f(T/T_i, H/H_i) \quad (2)$$

for a solution of single impurities[20,21] interacting only with the conduction electrons, where T_i and $H_i \equiv k_B T_i/\mu_B$ characterize the strength of the moment–conduction-electron interaction (e.g., the Kondo or localized-spin-fluctuation temperature and field).

It is of considerable interest to extend high-H magnetization studies in the spin-glass regime to a variety of transition-metal–base systems in order to better understand magnetic interactions in more complex materials where the applicability of the s-d model or the related[22] Anderson band-mixing model[23] is questionable.[24] Aside from "giant moment" magnetization studies on exchange-enhanced Pd-[25,26] and Pt-[27] base alloys, and recent work on Mo-Fe,[28] very little information has thus far been published. In addition, it is of value to interrelate $\Delta M(H,T)$ behavior with the character of the conduction-electron–localized-moment interaction as indicated by measurements of electrical resistivity $\rho(T)$ and magnetoresistivity $\delta\rho(H)/\rho(H=0)$ on the same specimens as employed for the $\Delta M(H,T)$ measurements.

In the present paper,[29] we report the results of low-temperature $1.2 \leq T \leq 27$ K measurements of magnetization, resistivity, and magnetoresistivity in applied magnetic fields up to 135 kG on the transition metal Zr containing dilute additions of Mn at concentrations $0.052 \leq c \leq 0.31$ at.% ($520 \leq c \leq 3100$ ppm). The presently available $(H/T)_{max} = 112$ kG K^{-1} has allowed saturation of the localized-moment magnetization, thus allowing more definitive comparison with theories of magnetization[11,12] and magnetoresistance[30,31] behavior. In a subsequent paper,[32] we shall report a somewhat similar study of the rare-earth-moment system Zr-Gd.

II. SPECIMENS

The bcc (β) phase of Zr is stable from the melting point down to about 860 °C,[33] at which point it transforms martensitically to the low-temperature-stable hcp (α) phase.[34] Above the α-β boundary there is extensive solubility of Mn in bcc Zr, but below the α-β boundary, the equilibrium solubility of Mn in hcp Zr is severely restricted, and is probably less than 0.5 at.%.[33] However, as discussed[35] with respect to the rather similar Ti-base systems, dilute metastable hcp solid solutions can be formed by quenching the alloys to room temperature from the bcc-phase field, since at low enough solute concentrations the martensitic β to α transformation apparently goes to completion above room temperature. Reasonably direct evidence for this interpretation is provided by studies[36] of Curie-Weiss behavior in the low-magnetic-field impurity susceptibility $\chi_i \equiv \chi(\text{alloy}) - \chi(\text{host})$ of both quenched and annealed dilute alloys in the Ti-Mn system. Since Mn displays[36,37] a low-temperature localized magnetic moment in hcp but not bcc Ti, it can be inferred from the $\chi_i(c)$ measurements that hcp solid solutions of Mn in Ti are formed by quenching from the bcc phase at solute concentrations $c \leq 0.2$ at.%. [Here and below (where required to avoid confusion) c_a is the concentration in at.%, c_f the concentration in atomic fraction, c_{ppm} the concentration in parts per million.] In a somewhat similar way, the present saturation magnetization $\Delta M_{max}(c)$ and low-H susceptibility $\chi_i(c)$ study (Secs. IV B and IV C) shows that hcp solid solutions of Mn in Zr

TABLE I. Electrical resistivity in zero applied magnetic field.

(1) Specimen designation [a]	(2) c_{ppm} [b] Chemical analyses (ppm)	(2) c_{ppm} [b] From premelt weights (ppm)	(3) ρ(77 K) ($\mu\Omega$ cm)	(4) ρ(4.2 K) ($\mu\Omega$ cm)	(5) ρ(77 K) − ρ(4.2 K) ($\mu\Omega$ cm)	(6) $\frac{\rho(4.2\text{ K})}{\rho(77\text{ K})-\rho(4.2\text{ K})}$	(7) T_{min} [c] (K)
Zr No. 1	...	...	7.22	1.32	5.90	0.224	...
Zr–520 Mn	520 ± 26	500	8.27	2.39	5.88	0.407	7.7
Zr–900 Mn	900 ± 45	1000	8.66	2.74	5.92	0.462	8.0
Zr–1690 Mn	1690 ± 84	2000	9.18	3.29	5.90	0.558	8.5
Zr–3100 Mn	3100 ± 155	4000	11.13	5.12	6.01	0.853	9.4

[a] Zr-c_{ppm} Mn designates an alloy with c_{ppm} parts per million of Mn.

[b] c_{ppm}: Mn concentration in parts per million; $c_{ppm} = 10^4 c_a = 10^6 c_f$ where c_a and c_f indicate Mn concentrations in, respectively, at.% and atomic fraction.

[c] T_{min}: temperature at the resistivity minimum as read from Fig. 3.

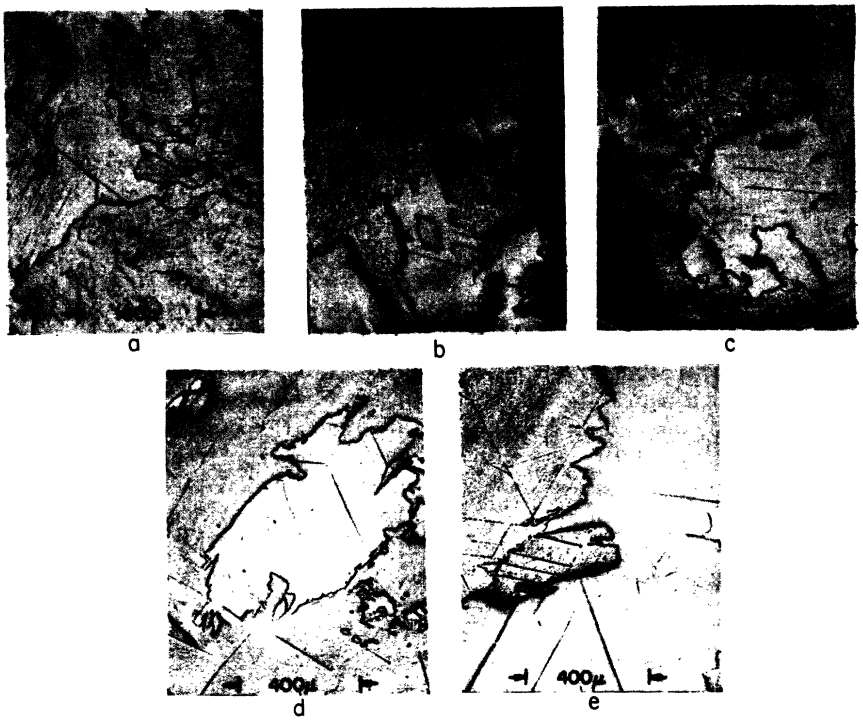

FIG. 1. Photomicrographs representative of (a) "pure" Zr specimen Zr No. 1, (b) Zr-520 ppm Mn, (c) Zr-900 ppm Mn, (d) Zr-1690 ppm Mn, (e) Zr-3100 ppm Mn.

are formed by quenching from the bcc phase at solute concentrations $c \leq 0.31$ at.%.

Crystal-bar "iodide process" Zr, produced by Foote Mineral Co., was utilized in the present study. A typical purity of 99.8 wt% (exclusive of Hf at ≈2000 ppm) was claimed by the manufacturer. A spectrographic analysis[38] of a piece from the particular bar used for the present specimens indicated impurity levels (in ppm) of Fe: 96; Cu: 13; Ti: <40; Co: <60; Ni: <75; Mn: <70; Cr: <40. Fortunately, the apparent possible $3d$-element contamination is not particularly serious here because χ_i ($\approx 10 < T < \approx 300$ K) measurements show that Fe[39] and Co,[40] do not display localized magnetic moments in hcp Zr, and[40] Cr displays only a weak saturation moment of about $0.2\mu_B$. The Mn was purchased from Gallard Schlesinger and was of nominal purity 99.99 wt%.

The alloys were consolidated under two-thirds of an atmosphere of "gettered" Ar in a laboratory arc-furnace utilizing a water-cooled copper hearth and a tungsten electrode. Each button was melted at least six times, with an inversion after each melt to promote homogeneity. For comparison with the alloys, a "pure" Zr button was also arc melted in a similar way from the same starting Zr bar, and specimen Zr No. 1 (Table I) was machined from the button. The resistivity ratio of this specimen was $\rho(273\text{ K})/\rho(4.2\text{ K}) = 30.1$.

Because of the possible loss of Mn due to its high vapor pressure, and because relatively high weight losses occurred during the arc melting, pieces from the Zr-Mn alloy buttons were chemically analyzed[41] for Mn content using a colorimetric technique with an accuracy of ≈ ±5%. Both the nominal concentrations as calculated from the starting weights and the chemically indicated con-

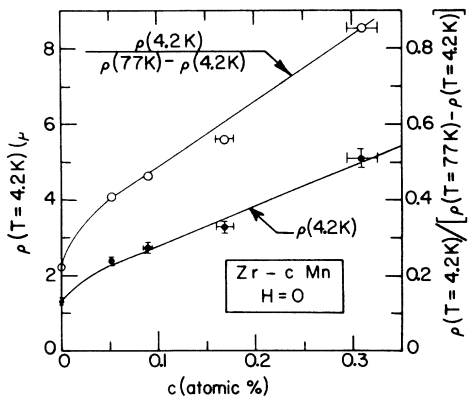

FIG. 2. Electrical resistivity at 4.2 K, $\rho(T = 4.2\text{ K})$, and the normalized electrical resistivity at 4.2 K, $\rho(4.2\text{ K})/[\rho(77\text{ K}) - \rho(4.2\text{ K})]$ vs Mn concentration c, all at zero applied magnetic field.

centrations are listed in Table I. Since the chemically indicated concentrations appear to be consistent with the measured saturation magnetizations ΔM_{max} (Sec. IV B), we have assumed these concentrations to be the true concentrations.

Sections of the arc-melted buttons adjacent to the sections cut for the specimens (Table I) were examined under a light microscope. The micrographs, shown in Fig. 1, all show an α-Zr "platelet" structure, typical of pure Zr which has been quenched from the β-phase field.[34]

Specimens were machined directly from the arc-cast buttons to a cylindrical form with hemispherical ends (so as to approximate ellipsoids of revolution), length ≈21 mm, diameter ≈1.5 mm, and demagnetizing coefficient[42] $D \approx 0.010$. Such geometry permits both magnetization and resistivity measurements. The specimens were subjected to a slow chemical etch, so as to remove an ≈0.13-mm surface layer and thus reduce surface impurities and strains induced by the machining.

Figure 2 and Table I show zero-H electrical resistivity data for the specimens. In Fig. 2, the upper curve shows the normalized resistivity $\rho(T=4.2\text{ K})/[\rho(T=77\text{ K})-\rho(T=4.2\text{ K})]$, which is independent of specimen geometry and potential-lead spacing. The lower curve shows the residual resistivity $\rho(T=4.2\text{ K})$ with ±5% vertical error bars reflecting primarily the geometric uncertainty in the potential lead separation and the average cross-sectional area $\langle A\rangle$ between the potential leads.[43] The horizontal error bars reflect the ±5% uncertainty in the chemical analyses. The nonlinearity of the curves at low c has been observed in other systems[16,44,45] and may be associated with impurity-impurity interactions. However, we cannot rule out the possibility that nonlinearity and scatter in the data of Fig. 2 reflect variations in the non-Mn impurity levels or in defect structures due, e.g., to slight variation in the arc-melting procedures employed in consolidating the different alloys.

A series of Zr-Mn specimens was also fabricated by sequentially arc melting, cold swaging, annealing, quenching, and then etching. However, both magnetization and residual resistivity measurements indicated that less Mn was retained in solution in these specimens, and that some impurity pickup may have occurred during the processing. Therefore, only data for specimens machined directly from the arc-cast buttons are discussed in the present paper.

III. APPARATUS AND METHOD

The magnetization data were obtained by measuring the flux change when a specimen was moved between two balanced series-opposition-wound search coils as previously described,[46] except that the earlier zero-restoring-torque galvanometer was replaced by an electronic voltage integrator (Thomas-Skinner, Model No. 7385). The output of the integrator was recorded on a time-base strip-chart recorder. The recorder deflection δ produced by translation of the specimen between the two coils was directly proportional to $\Delta\phi/R$ where $\Delta\phi$ was the total flux change in the search coil system and R was the total resistance in the search coil circuit consisting of R_i, the integrating resistor, and $R_c(H)$, the search-coil-system resistance. The deflection was corrected for the paramagnetic deflection due to the empty beryllium-copper specimen holder (directly proportional to H and ≈6% of the deflection due to the specimen Zr No. 1 at 4.2 K) and for the measured H dependence of the search-coil resistance $R_c(H)$ (normally a 1.5% correction at $H=135$ kG). The corrected deflection δ_c was then directly proportional to the specimen magnetization M in the spatially (±0.02% over the length of the coil system) and temporally (±0.01% over the time of the measurement) homogeneous applied field H. A calibration for each specimen of diameter d was obtained from a linear plot of δ_c/H vs d^2 as measured[46] for superconducting specimens (with lengths and diameters very similar to the present specimens) in the perfectly diamagnetic Meissner state ($B=0$) of known magnetization $M=-H/4\pi(1-D)$, where D is the specimen demagnetizing coefficient.

With the voltage integrator at maximum gain, the overall magnetometer sensitivity was such that $\delta_c(\text{mV}) \approx 30M$ (G). For specimens with $M>1$ G, measurements were usually made with reduced integrator gain (to reduce drift) such that $\delta_c(\text{mV}) \approx 3$ M (G). With this setting, δ could generally be read and reproduced to ≈±4% at $M=1$ G and ≈±0.5% at $M=5$ G. Some of this scatter may have been due to paramagnetic impurity particles in the He.[46] For a given specimen 8–12 deflections were usually measured and averaged at each (H,T) so as to reduce the random error. Absolute M values may be in error by ≈±10% due to approximate systematic errors of ±6% in the calibration procedure, ±1% in the specimen holder correction, and ±3% in the determination of the average specimen cross-sectional area[43] sensed by the search coils.

The cryogenic and magnetic systems, as well as the electrical resistivity measuring apparatus and method, were rather similar to those described earlier.[46-48] Data at $H<\approx 20$ kG were normally obtained with a low residual $H \approx 10$ G, 55-kG Nb-Zr superconducting solenoid,[46] while data at

$H > 20$ kG were normally obtained with a 140-kG, Nb_3Sn, superconducting solenoid[47,48] (Intermagnetics General) with a 2.125-in.-diam bore, a field homogeneity of better than 0.1% over a 3-cm-diam spherical volume, and a Cu-wire magnetoresistive field sensor. The latter was calibrated and axial field profiles were measured with a nominally 0.1% accurate null-deflection rotating-coil gaussmeter (Rawson Model No. 829S) which had been calibrated against the proton NMR frequency in glycerine.

IV. EXPERIMENTAL RESULTS

A. Electrical resistivity in zero applied magnetic field

Figure 3 shows zero-H electrical resistivity versus T curves for the "pure" Zr specimen, Zr No. 1 (labeled 0 ppm Mn), and for the Zr-Mn alloys of the present study. The measurements were made with a relative precision (for a given specimen) of about ±0.05%, employing a standard dc four-lead technique,[46] an adjustable-heat-leak probe,[35,46] and a Cu-to-Au (0.07-at.% Fe) thermocouple thermometer.[46] The salient features are the following.

(i) No resistance minimum is observed in the "pure" Zr specimen Zr No. 1 suggesting that possible $3d$-impurity contamination either in the starting or processed Zr does not give rise to localized magnetic moments of sufficient magnitude to perturb the present $\rho(H,T)$ or $M(H,T)$ measurements.

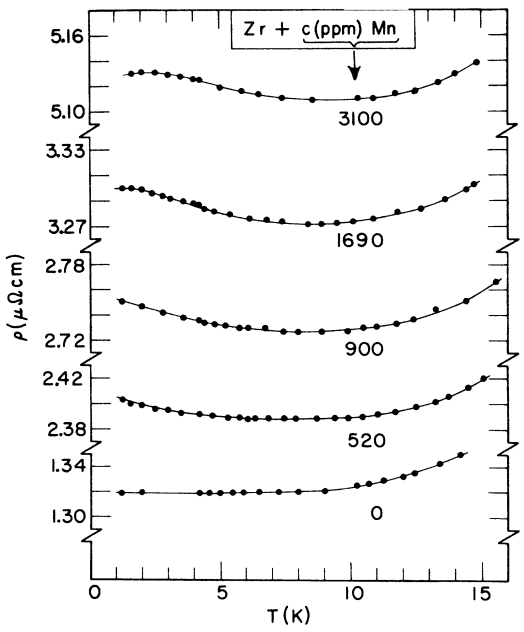

FIG. 3. Zero-H electrical resistivity ρ vs T for various concentrations of Mn in Zr. The curve marked "0" is that for the "pure" Zr specimen Zr No. 1.

(ii) Resistivity minima in the range 7–10 K are observed in the Zr-Mn alloys indicating that localized magnetic moments are associated with Mn when in solution in hcp Zr. This is consistent with earlier measurements[40] on a Zr–2000 Mn alloy (henceforth the designation $A - c_{ppm}B$ will be used to indicate c_{ppm} of B in A) which displayed Curie-Weiss behavior in the low-H impurity susceptibility χ_i ($\approx 10 < T < 300$ K), a resistivity minimum at $T \approx 8$ K, and negative magnetoresistance. The temperatures T_{min} at the resistivity minima are listed in Table I, column 7.

(iii) A peak in $\rho(T, H = 0)$ is observed for Zr–3100 Mn at $T_{max} = 2.0$ K. Such peaks are typically observed in alloys containing localized magnetic moments in the present concentration range and are commonly ascribed[49] to the influence of localized-moment-induced random internal molecular exchange fields H_m. Such fields act with progressively greater effectiveness as the temperature is lowered (H_m/T increased) to freeze out spin-flip scattering of conduction electrons from the moments, and thus counter the negative $d\rho/dT$ associated with Kondo or localized-spin-fluctuation single-impurity effects.

Studies of non-transition-metal base spin-glass systems[8] indicate that the maximum in $\rho(T)$ usually occurs at a temperature T_{max} somewhat above the "spin-freezing temperature" T_0, at which a cusp in the low-H impurity susceptibility χ_i occurs. The data of Fig. 3 thus suggest that the present investigation covers only the high-$T > T_0$ regime, as is also borne out by the (a) absence of irreversibility[8,50] in the low-H magnetization (Sec. IV B), and (b) absence of deviations from Curie-Weiss behavior[8] in the measured χ_i ($1.2 \leq T \leq 4.2$ K) of Zr–1690 Mn (Sec. IV C).

Figure 4 shows a semilog plot of $\Delta\rho/c$ vs T for the Zr-Mn alloys, where $\Delta\rho \equiv \rho(\text{alloy}) - \rho(\text{Zr No. 1})$. The irregularities apparent at $T > 9$ K probably reflect departures from Matthiessen's rule. The failure of the $\Delta\rho/c$ curves to superimpose shows that, with the possible exception of Zr–520 Mn, the data of Figs. 3 and 4 do not represent the single-impurity regime. The departure from single-impurity behavior might have been expected on the basis of comparison with other localized moment systems[8,20,21] at similar concentrations. The apparently anomalous ≈6% elevation of the $\Delta\rho/c$ curve for Zr–3100 Mn above that for Zr–1690 Mn is within the combined error of the measurement of $\Delta\rho/c$: ±5% for each alloy because of geometrical uncertainties which influence $\Delta\rho$,[43] and ±5% for each alloy because of the uncertainty in the chemical analysis determining c.

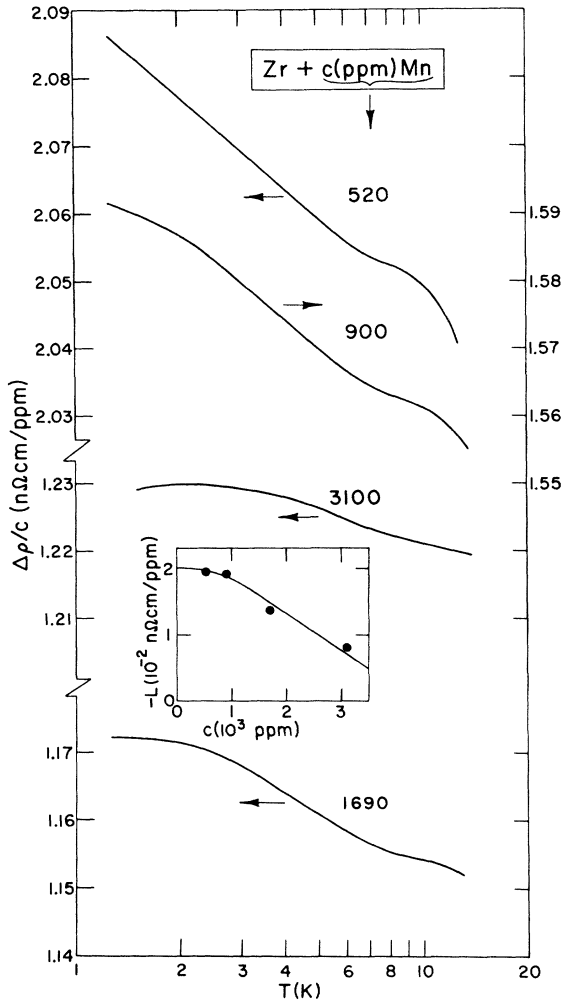

FIG. 4. Semilog plot of the specific impurity resistivity $\Delta\rho/c \equiv [\rho(\text{alloy}) - \rho(\text{Zr No. 1})]/c$ vs T for various concentrations c of Mn in Zr. The inset shows the slope L [Eq. (13)] of the $\Delta\rho/c$ vs ln T curves vs c.

A linear fit to the Zr-520 Mn data of Fig. 4 yields

$$\Delta\rho(1.2 \leq T \leq 5.8\ \text{K})/c = K + L \ln T, \tag{3}$$

with

$$K = 2.1\ \text{n}\Omega\ \text{cm/ppm}, \tag{4}$$

$$L = -1.9 \times 10^{-2}\ \text{n}\Omega\ \text{cm/ppm}. \tag{5}$$

The inset of Fig. 4 shows L vs c and suggests that Eq. (5) approximates the single-impurity limit L_0 obtained by extrapolation to $c = 0$. [The fact that $\Delta M(H)$ for Zr–520 Mn (Sec. IV B) is close to the free-spin Brillouin magnetization also suggests an approach to the single-impurity limit.] Equation (5) may be compared with the apparent single-impurity values (L_0 in 10^{-2} nΩ cm/ppm followed by the c_{ppm} of the specimen measured in parentheses): Au-Mn, −1.2(25) (Ref. 51); Ag-Mn, 0.72(57) (Ref. 45); Cu-Mn, −3.5(75) (Ref. 52); Zn-Mn, −20(23).[53] According to current theory,[54] L_0 is influenced by the non-exchange impurity scattering potential V. Thus L_0 can be used in only a very rough way[55] to estimate the exchange interaction potential J_ρ of relevance to the zero-H resistivity.[56]

Merely suggestive four-parameter fits of $\Delta\rho(T)/c$ is given by the Hamann-Fischer formula[54] (which included nonexchange scattering) to Eqs. (3)–(5) can be obtained. Assuming a constant ratio A_0/A_d of non-d-wave to d-wave nonexchange scattering of 0.5, fits can be obtained with the following triads of T_K, ρ_{du}/c (nΩ cm/ppm), and δ_v; 0.001 K, 3.5, 38°; 0.01 K, 3.2, 40°; 0.1 K, 3.0, 41°; 1.0 K, 2.9, 42°.[58] Here ρ_{du}/c is the unitary limit for d-wave scattering, δ_v is related to V through the relationship $\tan\delta_v \approx \pi N(0)V$ [$N(0)$ is the density of states], and T_K is the Kondo temperature. These values may be compared with the parameters $\rho_{du}/c \approx 2.0$ nΩ cm/ppm, $25.7° \leq \delta_v \leq 39.5°$, $0.03 \leq A_0/A_d \leq 0.89$, and $0.88 \leq T_K \leq 34$ K, implied by more legitimate fits[20] of the same equation[54] to $\Delta\rho(T)/c$ data over many decades of T for various noble-metal hosts containing Fe and Cr impurities. The exchange parameter J_ρ enters the expression for $k_B T_K \approx \epsilon_F \exp[-1/|\tilde{J}_\rho| N(0)]$, where ϵ_F is the Fermi energy and $\tilde{J}_\rho \approx J_\rho \cos^2\delta_v$. Using[60] $\epsilon_F = 8.2$ eV and interpreting $N(0)$ as a bare density of states[59] $N_b(0) \approx 0.26$ single-spin-states $\text{eV}^{-1}\text{atom}^{-1}$, the $T_K(\tilde{J}_\rho)$ and $\tilde{J}_\rho(J_\rho, \delta_v)$ equations, together with the present fit-determined pairs (T_K, δ_v) indicated above yield

$$|J_\rho| = 0.33,\ 0.40,\ 0.49,\ 0.60\ \text{eV} \tag{6}$$

(for, respectively, $T_K = 0.001$, 0.01, 0.1, 1.0 K), as derived from the $\Delta\rho(T, H = 0)$ data. Since the fits are relatively insensitive to T_K and the $\Delta\rho(T, H = 0)$ data for Zr–520 Mn may not adequately approximate the single impurity limit, the J_ρ values of Eq. (6) constitute only order-of-magnitude estimates at best, but are nevertheless within a factor of 4 of the J values estimated from the magnetization [Eq. (28)] and magnetoresistance [Eq. (35)]. More definitive studies with lower Mn concentrations, higher purity starting Zr, and lower measurement temperatures would be desirable for a proper assessment of the single-impurity regime.

The positive curvature of the $\Delta\rho/c$-vs-ln$T$ curve for Zr–520 Mn in Fig. 4 at $6 \leq T \leq 9$ K suggests that the curve may represent the high-T side of a Kondo step[58] with $T_K < 1$ K. This assessment is consistent with the lack of deviation from Curie-Weiss behavior in the impurity susceptibility of Zr–1690 Mn at $1.2 \leq T \leq 4.2$ (Sec. IV C), and with

the relatively low exchange interaction parameters $J \approx 0.2-0.5$ eV indicated by the magnetization and the magnetoresistance (Sec. V).

Table II, column 10, compares the present only roughly gauged $T_K < \approx 1.0$ K value for Zr-Mn with T_K values as estimated by other workers for non-transition-metal hosts containing Mn.

B. Magnetization

Figure 5 shows $M(H, T = 1.2\ \text{K})$ for the Zr-Mn alloys and $M(H, T = 4.2\ \text{K})$ for the "pure" Zr specimen Zr No. 1 (labeled 0 ppm Mn). The linearity of $M(H)$ for Zr No. 1 is consistent with the absence of resistivity minimum evidence (Fig. 3) for $3d$ localized moments and also indicates that f-shell moments, which may affect M (and the magnetoresistance) without producing a resistivity minimum in Zr,[32] are essentially absent. The presently measured 4.2 K volume susceptibility $\chi \equiv M/H = 9.0 \times 10^{-6}$ emu/cm^3 (dimensionless[61]) $= 1.2 \times 10^{-4}$ emu/mole (using $V_m = 13.88$ cm^3/mole[59]) is somewhat higher than the literature values for polycrystalline Zr (all in 10^{-4} emu/mole): $\chi(T = 20\ \text{K}) = 1.11$,[62] $\chi(T = 0\ \text{K}) = 1.1$,[63] $\chi(T = 20\ \text{K}) = 1.06$.[64] The latter value is calculated from anisotropic $\chi_{\parallel} = 1.47$ and $\chi_{\perp} = 0.86$ as measured[64] for a Zr single crystal, assuming random crystallite orientations so that $\chi = (\frac{1}{3})\chi_{\parallel} + (\frac{2}{3})\chi_{\perp}$ where $\parallel$ and $\perp$ mean, respectively, parallel and perpendicular to the hexagonal crystal axis. It is possible that a degree of preferred crystalline orientation (H parallel to hexagonal axis) exists in the present arc-cast specimen so as to account for the present relative high χ(Zr) value.

Figure 6 shows the Mn-induced impurity magnetization $\Delta M(H, T = 1.2\ \text{K}) \equiv M(\text{alloy}) - M(\text{Zr No. 1})$. We have assumed that M(Zr No. 1) is independent of T in the range $1.2 \leq T \leq 4.2$ K and have utilized the 4.2 K curve of Fig. 5 for $M(H$, Zr No. 1) at all $T \leq 4.2$ K. The curves of Fig. 6 show that as Mn concentration increases, the H required to saturate ΔM increases, until at 3100-ppm Mn the saturation field $H_s \approx 130$ kG ($H_s/T \approx 108$ kG/K). Such reluctance of localized moments to saturate in high (H/T) has been observed in both the moment-moment interaction regime[1-7,25-28] and in the apparent single-impurity regime[16,65,66] at $T < \approx T_i$ and $H < \approx H_i$, where moment–conduction-electron interaction inhibits free-spin behavior.[20,21]

The apparent slight negative slope in $\Delta M(H, T = 1.2\ \text{K})$ for Zr-900 Mn at $H > 80$ kG also appears at higher $T = 2, 4$ K and is probably an artifact of the measurement. Since $\Delta M \equiv M(\text{alloy}) - M(\text{Zr No. 1})$, the discrepancy could be accounted for by (a) a combined 8% error in the determination of the average cross-sectional areas of the Zr-900 Mn and Zr No. 1 specimens (although a combined maximum 6% error is estimated[43]), (b) a difference in preferred crystalline orientation[64] of Zr–900 Mn and Zr No. 1 such that the Zr susceptibility is less in the former. Effect (b) would cause a negative slope in $\Delta M(H$, Zr–900 Mn) above the H required to saturate the Mn moments in Zr-900 Mn. A Mn-induced decrease in the Zr susceptibility (due, e.g., to conduction electron spin polarization, or changes in the shape or filling of the Zr d-band) such as to give the negative slope seems unlikely in view of the absence of negative slope in the other Zr-Mn specimens. In order to avoid possible confusion and misinterpretation, the negative slope $M(H)$ data for Zr–900 Mn have not been shown in Figs. 9, 10, and 17.

Figure 7 shows $\Delta M_{\max}(T = 1.2\ \text{K})$ vs c_a for Zr-Mn alloys. The flatness of the high-H $\Delta M(H)$ curves of Fig. 6 suggests the identification of $\Delta M_{\max}$ with the saturation magnetization

$$\Delta M_{\max} = ngS\mu_B = (N_a V_m^{-1} c_f) g S \mu_B , \tag{7}$$

where n is the volume density of solute atoms, g is the Landé splitting factor [we make the usual assumption throughout this paper that for Mn in metallic solution the orbital contribution L is quenched so that $J = S$ (where L, J, and S are, respectively, orbital, total, and spin angular momentum quantum numbers)], μ_B is the Bohr magneton, N_a is Avogadro's number, and V_m is the molar volume. From Eq. (7),

$$S = (\Delta M_{\max}/c_f)[V_m/(N_a g \mu_B)]. \tag{8}$$

Insertion of the measured slope $\Delta M_{\max}/c_f = 1.58 \times 10^3$ G from Fig. 7 into Eq. (8), along with[59] $V_m = 13.88$ cm^3/mole for hcp Zr yields a best fit

$$S[\Delta M_{\max}(\text{fit})] = 1.96 \pm 0.2, \tag{9}$$

where the error limits reflect primarily the ±10% uncertainty in the absolute M determination (Sec. III). Equation (9) may be compared with the

$$S[\chi_i(\text{high } T)] = 1.75, \tag{10}$$

indicated by previous χ_i ($\approx 10 < T < 300$ K) measurements[40] on a nominal Zr–2000 Mn specimen, which yielded a $3.5\mu_B$ saturation moment from a Curie–Weiss-law fit; with the $S[\chi_i(\text{low } T)] = 2.00$ indicated by the present χ_i ($1.2 \leq T \leq 4.2$ K) measurements on Zr–1690 Mn [Eq. (14a)]; and with the value

$$S[\text{free } 3d^5 \text{ ion } (Mn^{2+})] = \tfrac{5}{2}. \tag{11}$$

The relatively low value of Eq. (10) may be due to an overestimate of the Mn concentration which was based[40] on the premelt weights. According to the Anderson[23] model, the differences between Eqs. (9), (10), (13), and Eq. (11) may be attributed to band mixing of the d-shell ionic states.

TABLE II. Magnetization data and parameters for various metals containing Mn in dilute solution.

(1) Alloy designation [a]	(2) c_f [b] (units of 10^{-4})	(3) n [c] (10^{19} cm^{-3})	(4) ΔM_{max} [d] (G)	(5) M_{bs} [e] (μ_B/Mn atom)	(6) S [f]	(7) ΔM_∞ [g] (G)	(8) V_0 [h] (10^{-37} erg cm^3)	(9) $\lvert J_{RKKY}\rvert$ [i] (eV)	(10) T_K [j] (K)	(11) χ_i [k] (T = 4.2 K) (units of 10^{-5})
Zr–520 Mn	5.2	2.26	0.77	3.67	1.83	...	...		$<\approx 1.0$	2.35
Zr–900 Mn	9.0	3.90	1.30	3.60	1.80	...	...		...	4.22
Zr–1690 Mn	16.9	7.33	2.64	3.88	1.94	2.84	2.7	0.5	...	8.12
Zr–3100 Mn	31.0	13.44	4.97	3.98	1.99	5.38	2.7	0.5	...	14.97
Au-Mn	...	...	...	4.50 [l]	2.25 ± 0.1 [m]	...	2.4 ± 0.3 [m]	0.9 ± 0.1 [m]	<0.02 [n] $\approx 10^{-13}$ [o]	...
Ag-Mn	...	...	...	3.90 [l]	1.95 ± 0.1 [m]	...	3.5 ± 0.4 [m]	1.1 ± 0.05 [m]	$0.01 - 0.04$ [p] ≈ 0 [q] $<10^{-16}$ [r]	...
Cu-Mn	...	...	...	3.76 [l]	1.88 ± 0.05 [m]	...	7.5 ± 0.9 [m]	2.2 ± 0.15 [m]	0.01 [s]	...
Zn-Mn	...	...	...	2.40 [l]	1.2 ± 0.1 [m]	...	20 ± 3 [m]	2.6 ± 0.4 [m]	1.0 [s]	...

[a] Zr-c_{ppm} Mn means c_{ppm} of Mn in Zr (all entries for these alloys are as determined in the present work); A-Mn means a dilute solution of Mn in A.
[b] $c_f \equiv$ atomic fraction $= 10^{-6}\, c_{ppm}$.
[c] $n \equiv$ atomic concentration of Mn $= (N_a/V_m)c_f = 0.4337 \times 10^{23}\, c_f$.
[d] Maximum high-H impurity magnetizations from Fig. 6.
[e] Saturation magnetization = maximum high-H impurity magnetization in μ_B/Mn atom $= \Delta M_{max}/n\mu_B$.
[f] Spin angular momentum quantum number $= M_{bs}/g$.
[g] Impurity magnetization linearly extrapolated $[\Delta M(H^{-1} \to 0) = \Delta M_\infty]$ in Fig. 18.
[h] RKKY coefficient obtained from $M(H^{-1})$ as explained in the text.
[i] RKKY exchange interaction parameter obtained from V_0 as explained in the text.
[j] Kondo temperature.
[k] Impurity susceptibility.
[l] From $M_{bs} = gS = 2S$, using S of column 6.
[m] From Reference 1.
[n] P. E. Lagendijk, L. Niesen, and W. J. Huiskamp, Phys. Lett. A 30, 326 (1969).
[o] Reference 51.
[p] Reference 45.
[q] J. C. Doran and O. G. Symko, Solid State Commun. 14, 719 (1974).
[r] Reference 57.
[s] Reference 20.

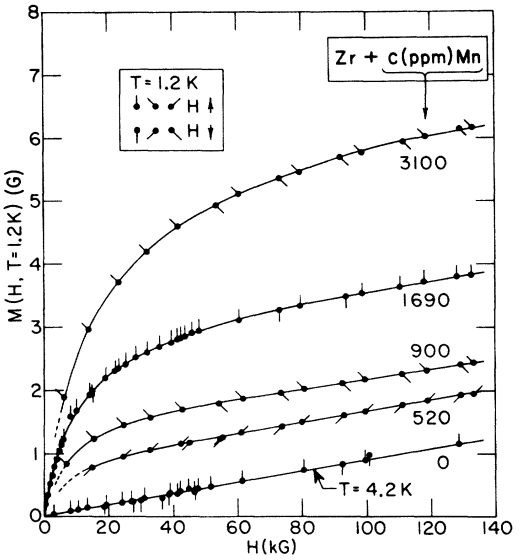

FIG. 5. Magnetization M at 1.2 K, $M(H, T=1.2\text{ K})$, vs applied magnetic field H for various concentrations c of Mn in Zr. The curve marked "0" is that for "pure" Zr specimen Zr No. 1 measured at $T=4.2$ K. For clarity not all data points at low H have been plotted.

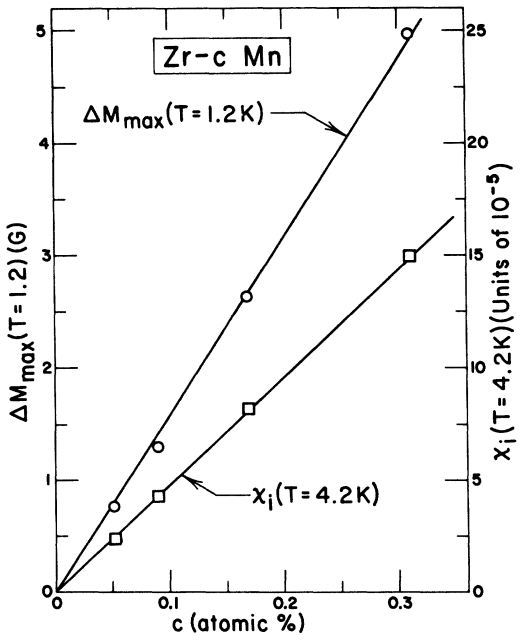

FIG. 7. Maximum impurity magnetization at 1.2 K (from Fig. 6), $\Delta M_{\max}(T=1.2\text{ K})$, vs Mn concentration c. Interpreting $\Delta M_{\max}$ as the saturation magnetization, the slope of the straight-line fit implies $S=1.96\pm0.2$ [Eq. (9)] as explained in the text. Also shown is the low-H impurity susceptibility $\chi_i=\lim_{H\to0}(\Delta M/H)$ vs Mn concentration c at 4.2 K. The slope of straight-line fit implies $S=2.01$ [Eq. (15)] as explained in the text.

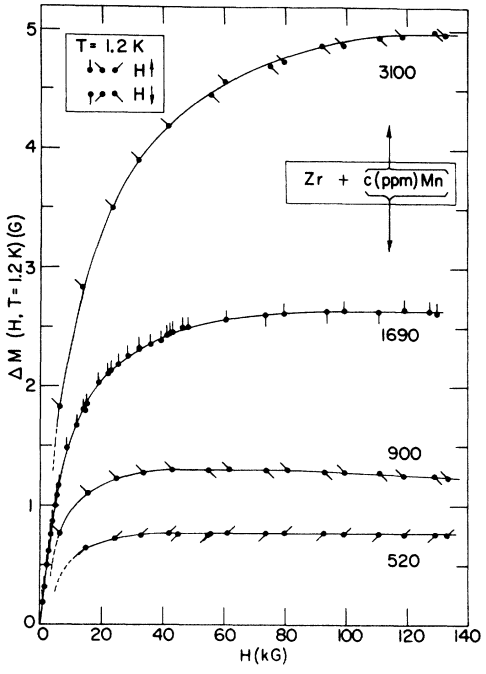

FIG. 6. Impurity magnetization $\Delta M \equiv M(\text{alloy}) - M(\text{Zr No. 1})$ at 1.2 K vs applied magnetic field H for various concentrations c of Mn in Zr. For clarity not all data points at low H have been plotted.

The measured values of S for Mn in various non-transition-metal solvents where $1.2\leq S\leq 2.25$ are listed in Table II.

Figure 8 shows the impurity magnetization (measured in μ_B/Mn atom) $M_b=\Delta M/n\mu_B$ as measured at 4.0 K and 1.2 K for Zr-1690 Mn and Zr-3100 Mn. The lower concentration alloy curves are not shown because their slightly lower measured S values (column 6, Table II) obscure comparison with $S=2$ Brillouin curves $M_{Bb}=gSB_s(gS\mu_BH/kT)$ shown in the figure. The $M_b(H)$ curves of Fig. 8 do not obey the single-impurity scaling relation Eq. (2), since $M_b\propto\Delta M/c$ is a function not only of H and T but also of c. A similar failure to display single-impurity behavior has been discussed with regard to the $\Delta\rho/c$-vs-T curves of Fig. 4.

Figure 9 shows $\Delta M(H/T)$ for Zr-Mn alloys. For comparison, the free-ion Brillouin curves for each alloy

$$M_B(H/T)=ngS\mu_BB_s(gS\mu_BH/k_BT), \qquad (12)$$

are shown for the particular value of S determined from the saturation magnetization and listed in column 6 of Table II. The primary features of these curves are the following.

(a) For $c\leq 900$ ppm, ΔM scales as (H/T) and is

in good agreement with the free-spin Brillouin magnetization. Similar agreement has been observed[3] for a Au–54-Mn specimen at $H \leq 50$ kG, and $1.7 \leq T \leq 4.2$ K. Such free spin behavior might be expected at $T \gg T_i, T \gg T_0$ (or at $H \gg H_i$, $H \gg H_0$) where T_i and $H_i \equiv k_B T_i/\mu_B$ characterize the strength of the impurity moment-conduction electron interaction and T_0 and H_0 characterize the strength of the moment-moment interaction.

(b) For $c \geq 1690$, the approach of the magnetization curves to saturation with increasing (H/T) is slower than indicated by the free-ion Brillouin curves—an effect which becomes more prominent as c is increased. This suggests net antiferromagnetic interactions which increase with c.

(c) For $c \geq 1690$, the approach of the magnetization to saturation with increasing H/T becomes progressively slower as T is reduced. This feature appears to be generally characteristic of localized moment magnetization in both the moment-moment interaction[1-7] and single-impurity $(T < \approx T_i)$[66] regimes. In the former case such behavior is apparently due to the more effective locking of moments by internal fields H_m at lower T (higher H_m/T).

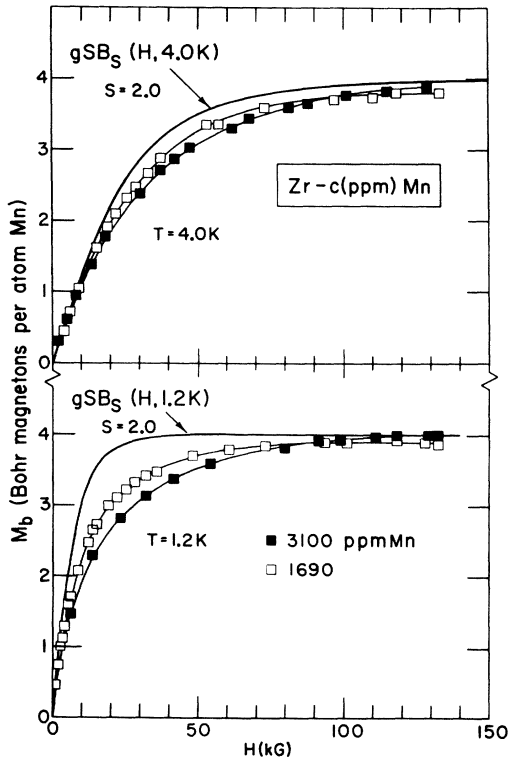

FIG. 8. Impurity magnetization in Bohr magnetons per Mn atom M_b vs applied magnetic field H for the Zr-Mn specimens containing 1690- and 3100-ppm Mn. For comparison, the Brillouin-function magnetizations $gSB_S(H/T)$ for $S=2$ are also shown.

Figure 10 shows $\Delta M/c$ plotted as a function of H/c at nearly constant T/c. The reasonably good superposition of data for different alloys on these curves indicates that BST scaling [Eq. (1)] is reasonably well obeyed. This, in turn, suggests that (a) the s-d RKKY model presupposed by Eq. (1) may have some degree of validity for the transition-metal host Zr, and (b) the present $M(H,T)$ data reflect primarily the influence of an oscillating long-range RKKY-type moment-moment interaction rather than a predominance of some near-pair coupling[21] or single-impurity coupling only to the conduction electrons. The minor influence of near-pair coupling (which might be especially important if chemical clustering[5,6,10] had occurred) is also indicated by the present absence of magnetization remanence and low-H hysteresis in either the magnetization or magnetoresistance (Sec. IV D). Such effects have been observed in[5] Cu-Fe and [5,67] Cu-Mn in the present c range. Recently BST scaling has also been observed[28] in the transition-metal-host Mo-Fe system at $0.84 \leq c \leq 1.42$-at.% Fe.

C. Low-H magnetic susceptibility

Figure 11 shows low-H $(H \leq 6$ kG) $\Delta M(H)$ curves in the range $1.2 \leq T \leq 4.2$ K for Zr-1690 Mn. Such

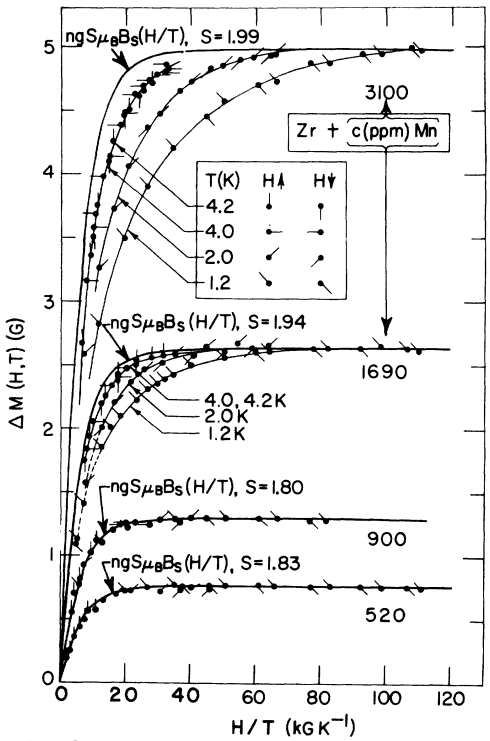

FIG. 9. The impurity magnetization $\Delta M(H, T)$ vs H/T for various concentrations c of Mn in Zr. For comparison, the Brillouin-function magnetizations $ng\ S\mu_B B_S(H/T)$ are also shown.

low-H data at closely spaced T intervals were not obtained for the other specimens. The lower-H linear sections of the curves (extended by dashed lines) define the low-H impurity susceptibility $\chi_i \equiv \lim_{H\to 0}(\Delta M/H)$.

Figure 12 shows χ_i^{-1} vs T for Zr-1690 Mn, where $\chi_i(T)$ values have been obtained from Fig. 11 as indicated above. The data fit a Curie-Weiss law

$$\frac{1}{\chi_i} = \frac{3k_B(T-\Theta)}{ng^2[S(S+1)]\mu_B^2}, \tag{13}$$

yielding the low-T susceptibility derived values

$$S[\chi_i(\text{low } T)] = 2.00, \tag{14a}$$

$$\Theta[\chi_i(\text{low } T)] = -0.37 \text{ K}. \tag{14b}$$

Equation (14a) is in good agreement with the $S = 1.96$ of Eq. (9) derived from a best fit to the saturation magnetization data.

The low-H impurity susceptibility χ_i was also measured at $T_m = 4.19$ K for the other Zr-Mn alloys, yielding values listed in Table II, column 11, and plotted in Fig. 7. The linearity of these points suggests that Θ is not markedly c dependent, although the accuracy of the present data and the possibility of a weakly c-dependent S (Table II, column 6) do not allow us to rule out the possibility that $\Theta \propto c$ as suggested by theory[11,12] for $T \gg \Theta$. Assuming, for the moment, that Θ is a constant Θ_c for all the alloys, Eq. (13) yields

$$[S(S+1)] = 3k_B(T_m - \Theta_c)g^{-2}\mu_B^{-2}(\chi_i/n).$$

Insertion of $T_m = 4.19$ K, $\Theta_c = -0.37$ K, $g = 2$, and the best fit $\chi_i/n = 1.10\times 10^{-24}$ cm^3 from Fig. 7 yields

$$S[\chi_i(\text{low } T, \text{fit})] = 2.01, \tag{15}$$

in good agreement with Eqs. (9) and (14a).

D. Magnetoresistance

Figure 13 shows longitudinal magnetoresistance curves $\delta\rho(H)/\rho_0$ for the pure Zr specimen Zr No. 1 and for the Zr-Mn alloys at $T \approx 1.4$, 4.2, 27 K. Here $\delta\rho(H) \equiv \rho(H) - \rho(H=0)$, $\rho_0 \equiv \rho(H=0)$, and "longitudinal" means that H is aligned parallel to the measuring current and to the longitudinal axis of the specimen. The experimental method[46-48] as applied to the present specimens allows a relative precision, for a given specimen, of about 3×10^{-4}. The salient features of these curves are the following.

(i) Zr-Mn alloys display negative magnetoresistance indicative[20,21] of interaction between conduction electrons and magnetic moments localized on Mn atoms. (The curves of Fig. 13 are consistent with earlier observations[40] of negative magnetoresistance at $H \leq 30$ kG, $T = 1.2$ K for a Zr-2000 Mn specimen.) Such negative magnetoresistance is commonly attributed[30,31] to the H-induced freeze-out of spin-flip scattering of conduction electrons from localized moments.

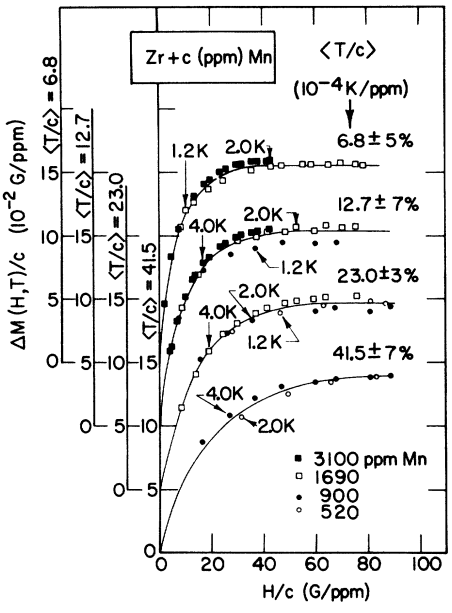

FIG. 10. Demonstration of the Blandin-Souletie-Tournier scaling $\Delta M/c = F(H/c, T/c)$. The specific impurity magnetization $\Delta M/c$ is plotted vs the "reduced" applied field H/c, at various nearly constant values of the "reduced" temperature T/c.

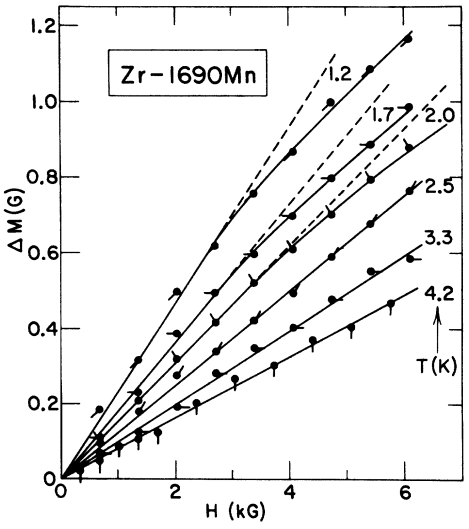

FIG. 11. Low-H impurity magnetization ΔM vs applied field H for the Zr-1690-ppm-Mn specimen at various temperatures T in the 1.2–4.2 K range. The low-H linear slopes determine the impurity susceptibility $\chi_i(T)$.

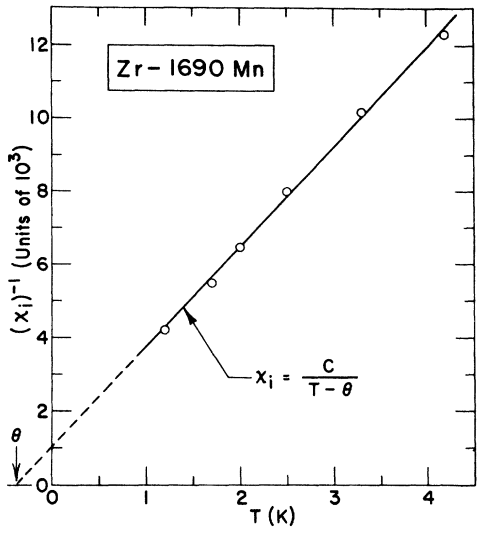

FIG. 12. Reciprocal impurity susceptibility χ_i^{-1} vs T for the Zr–1690-ppm-Mn specimen. The data fit a Curie-Weiss law $\chi_i = C/(T-\theta)$ with $\theta = -0.37$ K and C such that $S = 2.00$ [Eq. (14a)] as discussed in the text.

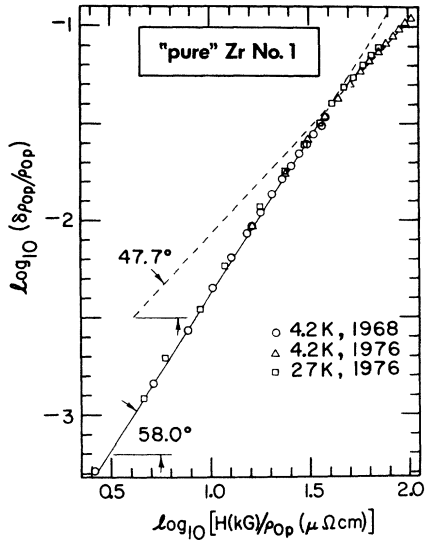

FIG. 14. Kohler plot of the magnetoresistance for the "pure" Zr specimen Zr No. 1. The logarithm of the normalized magnetoresistance $\delta\rho_p/\rho_{op}$ is plotted vs the logarithm of the normalized applied field H/ρ_{op}.

(ii) The negative magnetoresistance becomes more prominent as T is reduced, as is commonly observed in (a) the single-impurity regime,[52,68-70] and (b) the moment-moment interaction regime[67,70,72] at $T > T_{max} > T_0$ (see Sec. IV A 3), where internal molecular fields H_m are less effective in locking the moments.

The problem of the separation of the localized-moment-induced "spin-component" magnetoresistance $\delta\rho_s/\rho_0$ from the normal positive magnetoresistance $\delta\rho_n/\rho_0$ due to Lorentz-force bending of conduction-electron orbits can be troublesome.[73,74] However, the problem is less severe

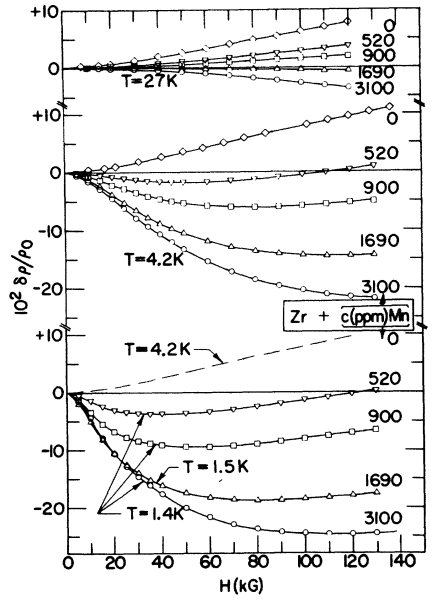

FIG. 13. Normalized magnetoresistance $\delta\rho/\rho_0$ vs applied field H at various temperatures T and for various concentrations c of Mn in Zr. Here $\delta\rho \equiv \rho(H) - \rho(H=0)$ and $\rho_0 \equiv \rho(H=0)$.

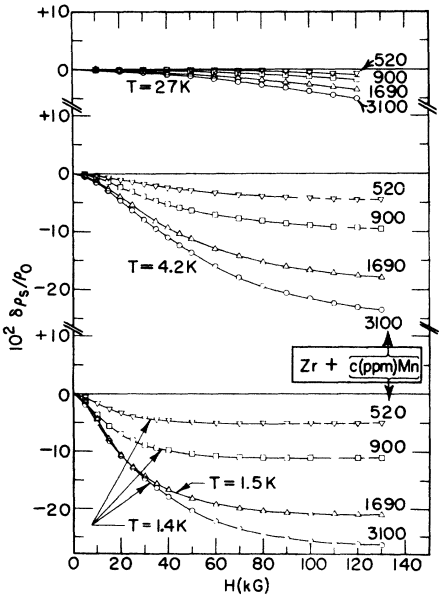

FIG. 15. Normalized spin-component magnetoresistance $\delta\rho_s/\rho_0$ vs applied field H at various temperatures T and for various concentrations c of Mn in Zr. Here $\delta\rho_s/\rho_0$ has been separated from the total magnetoresistance $\delta\rho/\rho_0$ of Fig. 13 by means of the Kohler plot, Fig. 14, as discussed in the text.

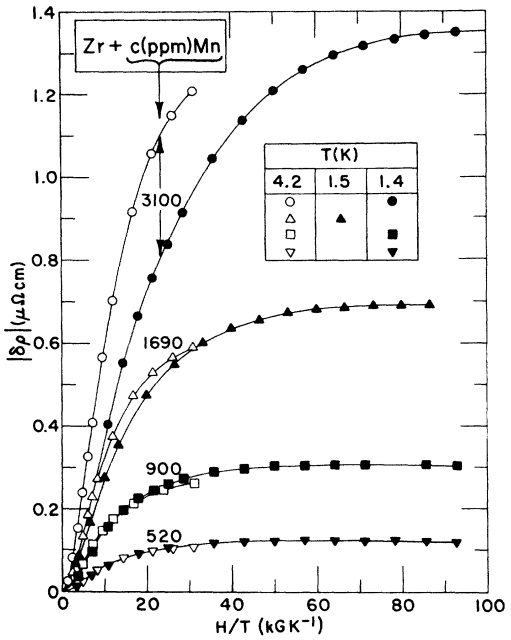

FIG. 16. Absolute value of the spin-component magnetoresistance $\delta\rho_s$ vs H/T at various temperatures T and for various concentrations c of Mn in Zr.

in the present case because (a) the nonmagnetic residual resistivities of the present Zr-Mn alloys are relatively high [≈ 1 $\mu\Omega$ cm (Table I, column 4 and Fig. 2) due to the relatively impure ($\approx$2000-ppm Hf) host Zr] so that $\delta\rho_n/\rho_0$ is relatively small, (b) at lower T and higher c, $\delta\rho_s/\rho_0$ is large in comparison with $\delta\rho_n/\rho_0$, and thus the latter can be satisfactorily approximated from a Kohler plot[74] of the magnetoresistance data for the "pure" Zr specimen Zr No. 1.

Figure 14 shows such a Kohler plot of $\log(\delta\rho_p/\rho_{0p})$ vs $\log(H/\rho_{0p})$ for specimen Zr No. 1. Here subscript "p" stands for "pure." Although not strictly correct,[73,74] we assume the validity of a "Matheissen's rule for magnetoresistance" such that for the Zr alloys

$$\frac{\delta\rho_n}{\rho_0}\left(\text{at}\,\frac{H}{\rho_0}\right)=\frac{\delta\rho_p}{\rho_{0p}}\left(\text{at}\,\frac{H}{\rho_{0p}}=\frac{H}{\rho_0}\right). \tag{16}$$

Thus the normalized spin-component magnetoresistance is taken to be

$$\frac{\delta\rho_s(H)}{\rho_0}=\frac{\delta\rho(H)}{\rho_0}-\frac{\delta\rho_p}{\rho_{0p}}\left(\text{at}\,\frac{H}{\rho_{0p}}=\frac{H}{\rho_0}\right), \tag{17}$$

where $\delta\rho(H)/\rho_0$ is the total measured magnetoresistance (Fig. 13), and the subtracted normal-state magnetoresistance component $\delta\rho_p/\rho_{0p}$ of Eqs. (16), (17) can be read directly from the Kohler plot of Fig. 14. The break in the Kohler-plot line at $(H/\rho_{0p})_B \approx 10^{1.6} = 40$ kG/$\mu\Omega$ cm between low-H [$\delta\rho/\rho_0 \propto (H/\rho_0)^{1.6}$] and high-$H$ [$\delta\rho/\rho_0 \propto (H/\rho_0)^{1.1}$] regions is characteristic[74] of many polycrystalline materials and may signify the onset of the high-H ($\omega\tau \gg 1$) regime where the magnetoresistance is determined by the topology of the Fermi surface, rather than the scattering processes. Therefore, Eq. (17) may be less reliable at $H/\rho_0 \geq (H/\rho_{0p})_B$.

Figure 15 shows $\delta\rho_s(H)/\rho_0$ for Zr-Mn alloys where the separation of the spin component $\delta\rho_s(H)$ has been effected by means of Eq. (17). Curves in the uncertain $H/\rho_0 \geq (H/\rho_{0p})_B$ region have been shown as dashed lines. Comparison of the spin-component $\delta\rho_s(H)/\rho_0$ curves of Fig. 15 with the total magnetoresistance $\delta\rho(H)/\rho_0$ curves of Fig. 13 (*these two figures are drawn with the same scales and placed adjacent with abscissas aligned for easier comparison*), shows that for Zr–1690 Mn and Zr–3100 Mn at $T \leq 4.2$ K, $\delta\rho_n/\rho_0 \leq 0.2\ \delta\rho_s/\rho_0$, so that small errors in $\delta\rho_n/\rho_0$ associated with the present inexact[73,74] Kohler treatment are not too important. On the other hand, for Zr-520 Mn at $T \leq 4.2$ K, $\delta\rho_n/\rho_0$ approximates $\delta\rho_s/\rho_0$ so that the latter is less reliable than in the more concentrated alloys. The Hurd-Alderson[74] iterative correction to the present Kohler treatment shifts the derived $|\delta\rho_s|$ by $\approx$8% or less in the presently investigated specimens.

Figure 16 shows $|\delta\rho_s|$ vs H/T, which may be compared with its magnetization counterpart ΔM vs H/T of Fig. 9. It is evident that $|\delta\rho_s|(H/T)$ is quite similar to $\Delta M(H/T)$: (a) the fields H_s required for saturation are about the same; (b) for $c \leq 900$ ppm, both scale as H/T; (c) for $c \geq 1690$ ppm, the departure from H/T scaling increases with c; (d) for $c \geq 1690$ ppm, the low-T curves fall below the high-T curves. Such similarity is not unexpected in view of the usual $|\delta\rho_s| \propto (\Delta M)^2$ observed in both the single-impurity[52] and impurity-impurity-interaction[67,75-78] regimes.

Figure 17(a) shows $-\delta\rho_s/c$ vs M_b^2 for Zr Mn alloys. Departure from the $|\delta\rho_s| \propto M_b^2$ relationship is especially apparent at the lower concentrations $c \leq 900$ ppm. The specific spin-component magnetoresistance at constant M_b^2 is c dependent in a direction opposite to that which might have been anticipated from results on Au Fe alloys,[69] where moment-moment interactions at $c = 1100$, 1900-ppm Fe appear to decrease $|\delta\rho_s|/c$ at constant H from its apparent single-impurity value.

V. COMPARISON OF EXPERIMENT AND THEORY

A. Magnetization

According to the high-temperature $T > T_0$ theory of Larkin and Khmel'nitskii,[11,12] the approach to saturation of the impurity magnetization ΔM is T independent and given by[79]

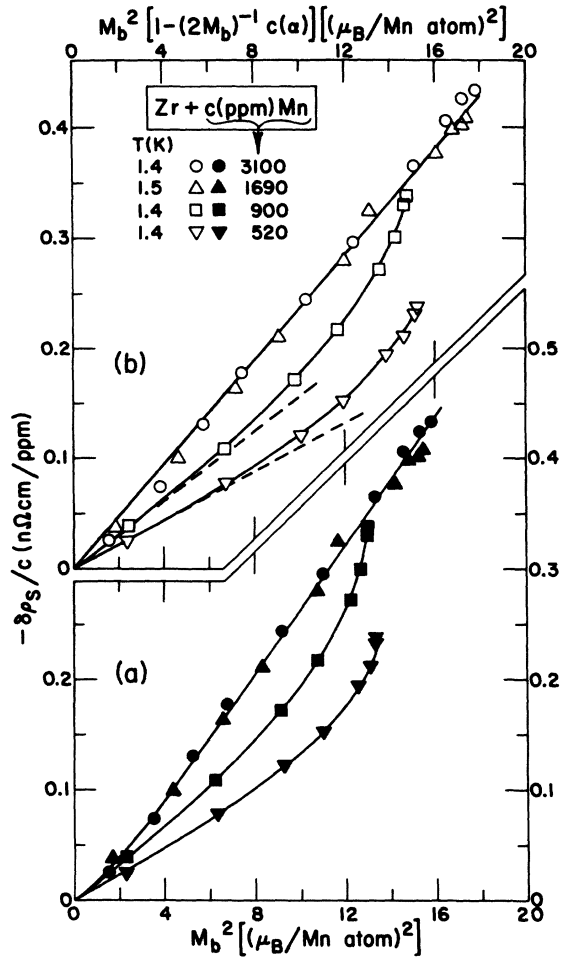

FIG. 17. Specific spin-component magnetoresistance $\delta\rho_s/c$ vs two different functions of the impurity magnetization M_b: (a) bottom, the square of the impurity magnetization; (b) top, the Béal-Monod and Weiner (Ref. 30) "freeze out factor" $A(\alpha)=M_b^2\,[1+2M_b c(\alpha)]$ as indicated in Eqs. (31) and (32) of the text. For $c\geq 1690$ ppm the measured values of $M_b(H, T=1.2\text{ K})$ have been slightly adjusted by linear-in-T interpolations between 1.2- and 2.0-K data so as to correspond to the temperatures indicated in the graph at which the magnetoresistance was measured. For $c\leq 900$ ppm, $M_b(H, T=1.4\text{ K})$ is as specified by the Brillouin magnetization $M_{Bb}=gSB_s(H,1.4\text{ K})$ with $S(900\text{ ppm})=1.80$, $S(520\text{ ppm})=1.83$, since these functions are shown to fit the data in Fig. 9.

$$\Delta M = ngS\mu_B[1-2(2S+1)nV_0/3g\mu_B H], \tag{18}$$

provided that (a) the moments are well defined, e.g.,

$$T\gg T_K \text{ or } H\gg H_K\equiv k_B T_K/\mu_B; \tag{19}$$

(b) $\Delta M(H,T)$ is measured in the high-H regime

$$H\gg k_B T/g\mu_B[H(\text{kG})\gg 7.4\ T(\text{K})] \tag{20}$$

and

$$H\gg nV_0/g\mu_B \quad [\text{for Zr: } H(\text{kG}) \gg 2.3\times 10^{34} c_{\text{ppm}} V_0\ (\text{erg cm}^3)]. \tag{21}$$

Here V_0 is defined by the RKKY expression (appropriate for $k_F r\gg 1$)

$$V_R(r)=V_0[\cos(2k_F r)]/r^3, \tag{22}$$

where k_F is the Fermi wave vector.

Figure 18 shows ΔM vs H^{-1} for Zr-Mn alloys in the (H,T) range $1.2\leq T\leq 4.2$ K, $20\leq H\leq 135$ kG. The linear T-independent approach to saturation predicted by Eq. (18) is not obeyed.

(a) The $\Delta M(H^{-1})$ curves bend over at the lowest H^{-1} (highest H) in accord with the Brillouin function ($c\leq 900$ ppm) or intermediate ($c\geq 1690$ ppm) between Brillouin-function and Larkin-Khmel'nitskii [Eq. (18)] behavior. This same type of departure from Eq. (18) has also been noted[3] for the relatively low V_0 (Table II, column 8) Au-Mn alloys at $c\leq 521$ ppm, $1.2\leq T\leq 4.3$ K, and $23\leq H\leq 50$ kG, although such alloys at higher $c\geq 1005$ ppm displayed linear $\Delta M(H^{-1})$ in the same field range. The present results suggest that it might be worthwhile to examine Au-Mn,[3] as well as alloys examined at $H\leq 50$ kG,[1,2,4] at higher H in order to check for a possible general breakdown of the linearity prediction of Eq. (18).

(b) The $\Delta M(H^{-1})$ curves are not T independent. A similar lack of T independence has been observed in many non-transition-metal–base alloys[1-4] and has been attributed to nonsatisfaction of Eq. (19)[2] or Eq. (20).[3]

Since, in the present alloys it appears that saturation is virtually complete at $H\leq 135$ kG, it seems unlikely that the failure of Eq. (18) can be attributed to nonsatisfaction of the high-H conditions of Eqs. (20), (21). However, Eq. (19) may not be well satisfied since, for T_K as high as 1.0 K, the H range 20–135 kG of Fig. 18 is such that $H\gtrsim H_K$ = 15 kG.

Although the Larkin *et al.*[11,12] theory does not seem to account for important features of the present $\Delta M(H^{-1})$ curves, it may be worthwhile to apply the theory in a rough way to the alloys for which $c\geq 1690$ ppm so as to obtain values of V_0 and J_{RKKY} which can be compared with similarly derived values[1-3] for non-transition-metal base alloys. Ignoring, for the present, the low-H^{-1} saturating portions of the $M(H^{-1})$ curves for Zr–1690 Mn and Zr–3100 Mn, the straight lines of Fig. 18 approximate the curves up to $H^{-1}\approx 3\times 10^{-5}$ G^{-1} ($H\approx 33$ kG) and extrapolate to "pseudosaturation-magnetization" values $\Delta M_\infty\equiv\Delta M(H^{-1}\to 0)$ as listed in Table II, column 7.

Following Smith *et al.*,[1-3] the straight lines of

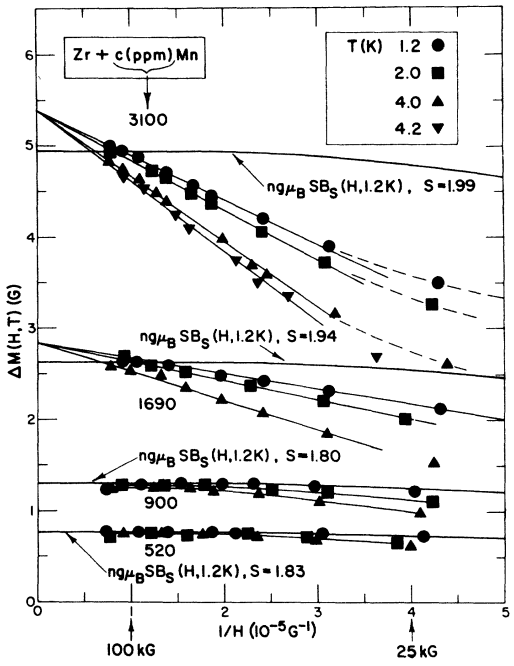

FIG. 18. Impurity magnetization ΔM vs the reciprocal applied field H^{-1} at various temperatures T and for various concentrations c of Mn in Zr. For comparison, the Brillouin function magnetizations $n_g S\mu_B B_s(H/T)$ are also shown. The straight line extrapolations to $H^{-1}=0$ represent behavior in accord with the high-H Larkin-Khmel'nitskii expression for $\Delta M(H^{-1})$ as explained in the text.

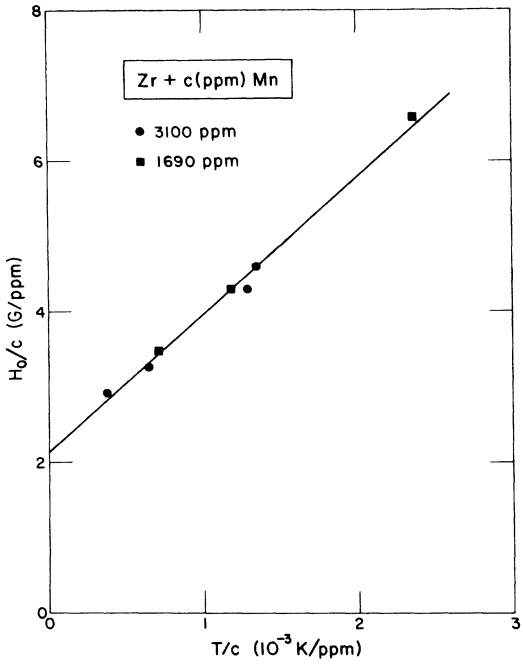

FIG. 19. "Reduced" slope H_0/c [see Eq. (23)] of $\Delta M(H^{-1})$ (straight-line fits in Fig. 18) plotted vs the "reduced" temperature T/c for the Zr–1690-ppm-Mn and Zr-3100-ppm-Mn specimens. The $T/c=0$ intercept [see Eq. (24)] implies an RKKY coefficient $V_0=2.7\times10^{-37}$ erg cm^3 as discussed in the text.

Fig. 18 can be expressed as

$$\Delta M=\Delta M_\infty[1-H_0(n,T)/H], \tag{23}$$

with

$$H_0(n,T)=Pk_BT+QnV_0. \tag{24}$$

Comparison of Eq. (18) with Eqs. (23), (24) shows that

$$Q=2(2S+1)/3g\mu_B. \tag{25}$$

Figure 19 shows H_0/c vs T/c for the Zr-Mn alloys. A linear relationship is obtained as observed by Smith[1-3] but contrary to other experimental[4] (Ag Mn) and theoretical[80] work. Linear extrapolations to $T/c=0$ yield

$$V_0=2.7\times10^{-37}\ \text{erg cm}^3 \tag{26}$$

as listed in Table II, column 8.

A value of the exchange interaction parameter J_{RKKY} relevant to the RKKY interaction[56] may be deduced from the V_0 value since[11,15,81]

$$V_0=(3Z)^2(\pi/2\epsilon_F)J^2_{\text{RKKY}}/(2k_F)^3. \tag{27}$$

Inserting values for Zr: $Z=4$, $\epsilon_F=8.2$ eV,[60] $k_F=1.73\times10^8$ cm^{-1},[59] $V_0=2.7\times10^{-37}$ erg cm^3 [Eq. (26)] into Eq. (27) yields

$$|J_{\text{RKKY}}|=0.50\ \text{eV}. \tag{28}$$

Considerable uncertainty (see *Note added in proof*) attaches to this estimate of J_{RKKY} because of (a) the apparent breakdown at low (H^{-1}) of Eq. (23) and hence the uncertainty in the derived V_0 [Eq. (26)], (b) the use of free-electron estimates[59] for Z and k_F in Eq. (27), and (c) the use of a band-structured calculated[60] ϵ_F in Eq. (27).

B. Magnetoresistance

According to the third-order perturbation analysis of Béal-Monod and Weiner[30,31] (BMW), valid for

$$T\gg T_K \quad\text{or}\quad H\gg H_K\equiv k_BT/\mu_B, \tag{29}$$

$$\delta\rho_s/c_f=-3\pi m^*V_A\epsilon_F\mathcal{J}^2(2e^2\hbar)^{-1}\times\{A(\alpha)[1+3Z\mathcal{J}[1.57+\ln(k_BT/2\epsilon_F)]]-3Z\mathcal{J}B(\alpha)\}, \tag{30}$$

where V_A is the volume per host atom, $\alpha\equiv g\mu_BH/k_BT$, m^* is the effective electron mass, $\mathcal{J}\equiv J_m/\epsilon_F$, J_m is the exchange interaction parameter relevant for magnetoresistance,[56] and all other parameters are as previously defined. Equation (30) is

valid in the single-impurity limit for arbitrary (H,T), provided that $|J_m|$ is much less than the nonexchange impurity scattering potential V (as appears to be the case for most alloy systems investigated to date[30,76-78]). Physically Eq. (30) expresses the magnetoresistance due to (a) H/T-induced freeze-out $[A(\alpha)$ factor] of single spin flip (first Born approximation $\mathcal{J}^2$ terms) and double spin flip (Kondo-type second Born approximation $\mathcal{J}^3$ terms), and (b) the H/T dependence of the second Born approximation scattering amplitude $[B(\alpha)\mathcal{J}^3$ term]. Expressing the impurity magnetization ΔM in terms of Bohr magnetons per Mn atom, $M_b = \Delta M/n\mu_B = g\langle S_z\rangle$, the $A(\alpha)$ and $B(\alpha)$ factors may be written (for $g=2$)

$$A(\alpha) = M_b^2[1 + (2M_b)^{-1}c(\alpha)], \tag{31}$$

where

$$c(\alpha) = \coth(\tfrac{1}{2}\alpha) - (\tfrac{1}{2}\alpha)[\sinh^2(\tfrac{1}{2}\alpha)]^{-1}, \tag{32}$$

and

$$\begin{aligned} B(\alpha) = {} & [S(S+1) - M_b^2 - (\tfrac{1}{2}M_b)\coth(\tfrac{1}{2}\alpha)] \\ & \times [I_1(\alpha) - I_1(0)] + (\tfrac{1}{2}\alpha)(\tfrac{1}{2}M_b)[\sinh^2(\tfrac{1}{2}\alpha)]^{-1} \\ & \times [I_2(\alpha) - I_2(0)], \end{aligned} \tag{33}$$

where $I_1(\alpha)$ and $I_2(\alpha)$, the same functions as given in an earlier treatment,[82] are presented graphically[30,82] with $I_1(0) = I_2(0) = -0.432$. For $\alpha > 10$, $I_1(\alpha)$ and $I_2(\alpha)$ vary essentially as $\ln H$, which replaces the $\ln T$ of the zero-H Kondo effect.

Insertion of ϵ_F, m^*, and $V_A = V_m/N_a$, for Zr,[59] into Eq. (30) yields

$$\begin{aligned} \delta\rho_s/c = -10.9\{ & \mathcal{J}^2 A(\alpha) + 3Z\mathcal{J}^3[1.57 + \ln(k_B T/2\epsilon_F)]A(\alpha) \\ & - 3Z\mathcal{J}^3 B(\alpha)\}\ \text{n}\Omega\,\text{cm/ppm}, \end{aligned} \tag{34}$$

where $A(\alpha)$ and $B(\alpha)$ may be determined from the measured magnetization $M_b(H,T)$ in accord with Eqs. (31)-(33).

If the $\mathcal{J}^3$ terms of Eq. (34) are neglected, then Eqs. (31), (34) indicate that $-\delta\rho_s/c$ should be proportional to $A(\alpha) \equiv M_b^2[1 + (2M_b)^{-1}c(\alpha)]$ rather than M_b^2. Fig. 17(b) shows $-\delta\rho_s/c$ vs $A(\alpha)$. As in Fig. 17(a), departure from linearity is especially apparent at the lower concentrations $c \leq 900$ ppm. The slopes of these curves (dashed lines for $c \leq 900$ ppm) yield [from Eq. (34) with $\mathcal{J}^3 = 0$] $|J_m(\mathcal{J}^3 = 0)| = 0.26$, 0.31, 0.39, 0.39 eV for, respectively, $c = 520$, 900, 1690, 3100 ppm. However, it is doubtful that much significance can be attached to these J_m values since (a) there seems to be little justification for ignoring the $\mathcal{J}^3$ terms in Eq. (34), and (b) Eq. (34) applies only to the single-impurity regime where J_m should be independent of c.

Figure (20) compares the observed specific magnetoresistance $\delta\rho_s/c$ with the complete Eq. (34)

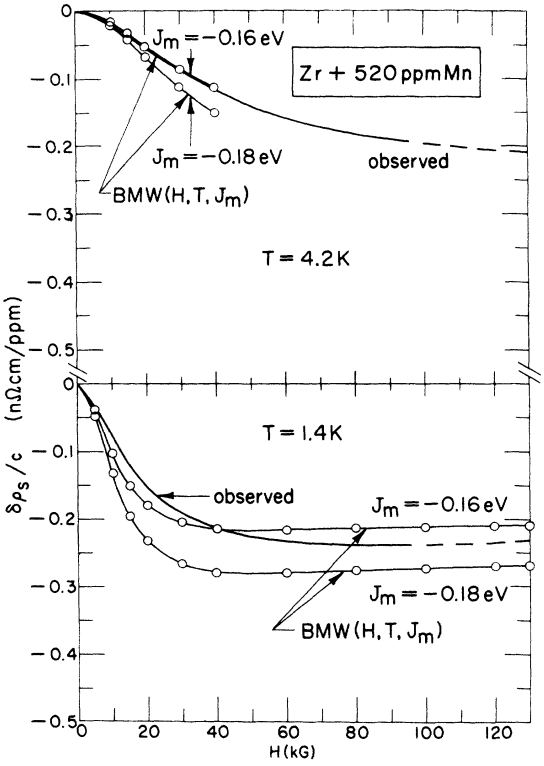

FIG. 20. Specific spin-component magnetoresistance $\delta\rho_s/c$ vs applied field H at $T = 4.2$ and 1.4 K for the Zr–520 -ppm-Mn specimen. The BMW curves show the predictions of the Béal-Monod and Weiner third-order perturbation theory with insertion of the presently measured magnetizations $M_b(H,T)$. The BMW ($T = 4.2$ K) curve is shown only for $H \leq 40$ kG because technical difficulties prevented the accurate measurement of M_b at higher H. The $M_b(H, T = 1.4)$ used in the BMW formula is as specified by the Brillouin magnetization $M_{Bb} = gSB_S(H, T = 1.4\text{ K})$ with $S = 1.83$, since this function is shown to fit the data in Fig. 9. The dashed portions of the observed $\delta\rho_s/c$ curves indicate regions over which separation of the spin component was effected by use of the Kohler plot (Fig. 14) at H/ρ_{ob} values above the high-H break in the plot of Fig. 14.

for the Zr–520 Mn alloy which most nearly approaches the single-impurity regime. For the highest $H \approx 130$ kG, where the convergence condition Eq. (29) is best satisfied, the BMW fit implies

$$J_m = -0.17\text{ eV}, \tag{35}$$

which is a factor of 3 less than the J_{RKKY} estimate of Eq. (28).

The $\delta\rho_s/c$ curves as predicted by BMW at $T = 1.4$ K, $H > 40$ kG where M_b is saturated (Fig. 6) display a small *positive* slope as emphasized by BMW.[31] This positive slope is due to the H dependence of the scattering amplitude,[31] and is also predicted by an S-matrix calculation,[83] but the

detailed physical mechanism which might be responsible for such a positive slope seems somewhat obscure. There is a slight positive slope for the observed $\delta\rho_s(H, T = 1.4\ \mathrm{K})/c$ at $H > 115$ kG but refined studies at still higher H appear to be needed to adequately investigate this aspect.

Figure 21 compares the observed specific magnetoresistance $\delta\rho_s/c$ with Eq. (34) for the Zr–3100 Mn alloy in which Mn-Mn interactions are most prominent, as indicated in Figs. 4, 6, 9, and 16. The apparent J_m values indicated by the BMW fits are not greatly different from Eq. (35).

VI. DISCUSSION AND SUMMARY

The present work attempts to shed some light on localized-moment interactions in a transition-metal host Zr, through the experimental investigation of high-H magnetization and magnetoresistance, low-H susceptibility, and zero-H electrical resistivity, all performed on the same specimens. The primary results are as follows:

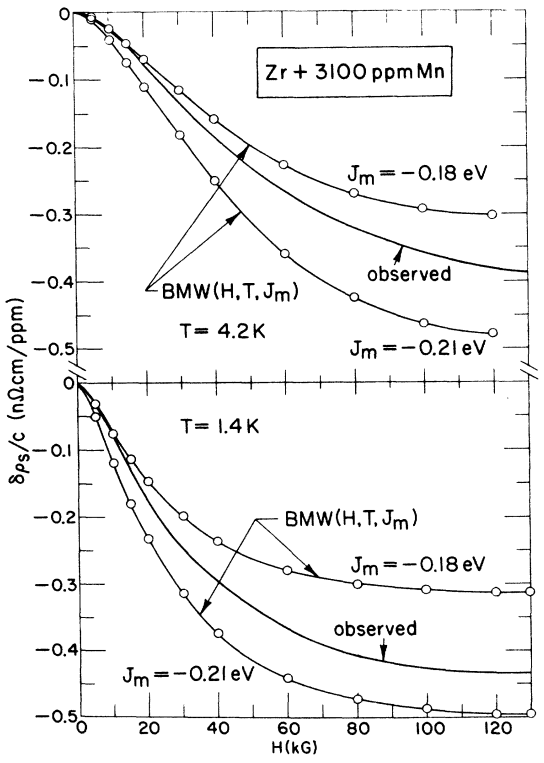

FIG. 21. Same as Fig. 20 except that the specimen is Zr–3100-ppm Mn and the measured $M_b(H, T)$ have been slightly adjusted by linear-in-T interpolations between 1.2- and 2-K data so as to correspond to the temperature at which the magnetoresistance was measured.

(a) The resistivity, magnetoresistivity, and magnetization measurements confirm the earlier indications[40] that Mn displays a localized magnetic moment when in solution in hcp Zr. The zero-H resistivity of the most dilute $c = 520$-ppm specimen suggests that the Kondo temperature $T_K < 1.0$ K, as is characteristic of noble-metal hosts containing Mn in dilute solution (Table II, column 10).

(b) Both the high-H magnetization and low-H susceptibility show that the spin S associated with Mn in dilute solution in Zr is 2.0 ± 0.2 [Eqs. (9), (14a), and (15)]. Similar S values are observed in Mn in solution in noble-metal hosts (Table II, column 6).

(c) The observation of a peak in the zero-H resistivity at $T_{max} \approx 2$ K for Zr–3100 Mn suggests[8] that the spin-freezing temperature T_0 (if it exists in Zr-Mn) is such that $T_0(c = 3100\ \mathrm{ppm}) < 2$ K. The Curie-Weiss behavior of the low-H susceptibility of Zr-1690 Mn at $1.2 \leq T \leq 4.2$ K indicates that $T_0(c = 1690\ \mathrm{ppm}) < 1.2$ K. These $T_0(c)$ limits suggest that $T_0(c)$ in Zr-Mn is lower than that observed in Cu-Mn,[8] but possibly similar to $T_0(c)$ as observed in Ag-Mn and Au-Mn.[8] Direct measurements of $T_0(c)$ in Zr-Mn by means of susceptibility and specific-heat measurements at $T < 1$ K are clearly desirable.[84] Such measurements, might also explore a possible confluence of spin-freezing and superconductive pair condensation at $T < T_c(\mathrm{Zr}) \approx 0.5$ K.

(d) The impurity magnetization $\Delta M(T = 1.2\ \mathrm{K})$ in Zr-cMn alloys saturates at fields $40 \leq H_s \leq 130$ kG (for $520 \leq c \leq 3100$ ppm). As far as we are aware, these are the first observations of magnetization saturation in relatively concentrated ($c > 500$ ppm) spin-glass systems above T_0.

(e) The impurity magnetization ΔM in Zr-c Mn at $520 \leq c \leq 3100$ obeys the BST[17,18] scaling $\Delta M = F(H/c, T/c)$ suggesting the presence of a long-range oscillating, RKKY-like Mn-Mn interaction in the transition-metal host Zr.

(f) The approach to saturation of the impurity magnetization ΔM in Zr-Mn differs from that predicted by the Larkin-Khmel'nitskii[11,12] theory since (a) the measured $\Delta M(H^{-1})$ is T-dependent as observed[1-4] in non-transition-metal-base alloys, and (b) the measured $\Delta M(H, T = 1.2\ \mathrm{K})$ saturates as indicated in (d) above instead of approaching saturation linearly in H^{-1} for $0 \leq H^{-1} \ll g\mu_B/k_BT$. The present work suggests that cutoff values in the molecular-field distribution may exist at $(H_m)_{max}$ on the order of $H_s(c)$ in the Zr-Mn alloys of this study. It is possible that the present relatively low $H_s(c)$ is associated with the relatively[85] high residual resistivities (Fig. 2 and Table I, column 4), since shortened electron mean free paths could result in a damping of the RKKY oscillations.[86] If such damping exists it is

apparently not of sufficient magnitude to destroy the BST scaling. Systematic studies of H_s and BST scaling as functions of nonmagnetic impurity doping would be desirable.

The insertion of physically required $(H_m)_{max}$ cutoffs into random-molecular-field theory has recently been considered by Klein, Fischer, and Riess.[80,87,88] However, their predicted[80] magnetization-approach-to-saturation is a low-T-limit expression for which the cutoff is believed[80] to be irrelevant. Their expression apparently agrees with the observations of Hou and Coles[4] on Ag-Mn, but seems to be at variance with the present work on Zr-Mn and with the measurements of Smith and co-workers[1-3] on Au, Ag, Cu, and Zn containing Mn.

(g) The value of the exchange interaction parameter $|J| \approx 0.2-0.5$ eV in Zr-Mn as suggested by high-field magnetization [Eq. (28)] and high-field magnetoresistance [Eq. (35)] is probably only of order-of-magnitude significance. As such it is comparable to similarly derived values for noble-metal hosts containing Mn in dilute solution (Table II, column 9).

(h) The spin-component magnetoresistance $\delta\rho_s$ of a localized-magnetic-moment metallic system has been examined, apparently for the first time, under conditions of impurity magnetization ΔM saturation (Figs. 6, 16, and 20). Concomitant saturations in $\delta\rho_s(H)$ and $\Delta M(H)$ are observed. Detection of the small positive slope in $\delta\rho_s(H)$ predicted by BMW[30,31] (Fig. 20) under conditions of magnetization saturation is probably beyond the resolution of the present experiment. Further measurements at higher fields in lower-Mn-concentration Zr-Mn and Zr-Hf-Mn alloys are planned to explore this interesting single-impurity prediction.

In general, the present work indicates that the localized-magnetic-moment and high-$T > T_0$ spin-glass behavior of Mn in the transition metal Zr is rather similar to that displayed by Mn in the noble metals Cu, Ag, and Au. However, a thorough comparison is prohibited by the dearth of data for the latter alloys at $H > 50$ kG. The present observations of relatively low-H saturation of the impurity magnetization do not appear to agree with current $T > T_0$ theory,[11,12] but it is presently unclear whether this type of high-H disagreement is a general property of spin glasses, or is peculiar to transition-metal–host systems or to systems with relatively short electron mean free paths.

It would appear that further high-H measurements over wider T ranges, which encompass both the frozen- and unfrozen-spin regimes in many different transition- and non-transition-metal–host spin-glass systems should be of value in elucidating the nature of localized-moment interactions in metals and, more generally, the "freezing" of random systems.[9]

Note added in proof. F. W. Smith (private communication) has pointed out to us that for transition metals it may be preferable to interrelate V_0 and J through the measured electronic specific-heat coefficient γ. Following, for example, A. A. Abrikosov [Sov. Phys.-Usp. 12, 168 (1969), Eq. (3)] and using the presently defined symbols and units, the V_0-J relationship may be written $J^2 = 2.23 \times 10^{37}\, V_0(1+\lambda)(\gamma V_m)^{-1}$, where $1+\lambda$ is the phonon enhancement factor. Taking $1+\lambda = 1.41$ for Zr from W. L. McMillan [Phys. Rev. 167, 331 (1968)]; V_0 from Eq. (26); and γ and V_m as in Ref. 59, we obtain $|J| = 0.47$ eV in agreement with Eq. (28).

ACKNOWLEDGMENTS

We should like to thank D. M. Sellman and P. Q. Sauers for their invaluable assistance in the early experimental work and in the preparation of specimens; E. Parry, R. A. Spurling, and C. G. Rhodes for their careful chemical and metallographic analyses; and M. W. Klein and F. W. Smith for helpful comments. One of us (R.R.H.) wishes to acknowledge the hospitality and helpfulness of the UCLA Physics Dept. and Solid State Group during a sabbatical period.

---

†Supported in part by NSF Grant Nos. DMR 75-09940 and 72-02935.

*Permanent address: Indiana University, Bloomington, Ind. 47401.

[1]F. W. Smith, Phys. Rev. B 14, 241 (1976), and references therein.

[2]F. W. Smith, Phys. Rev. Lett. 36, 1221 (1976).

[3]J. C. Liu, B. W. Kasell, and F. W. Smith, Phys. Rev. B 11, 4396 (1975).

[4]P. W. Hou and B. R. Coles, Phys. Rev. Lett. 35, 1655 (1975).

[5]J. M. Franz and J. D. Sellmyer, Phys. Rev. B 8, 2083 (1973).

[6]J. A. Careaga, B. Dreyfus, R. Tournier, and L. Weil, in *Proceedings of the Tenth International Conference on Low Temperature Physics*, edited by M. P. Malkov (Viniti, Moscow, 1967), p. 284.

[7]J. A. Careaga and R. Tournier, quoted in Ref. 18.

[8]For an experimental review see J. A. Mydosh, AIP Conf. Proc. 24, 131 (1975).

[9]For a theoretical review see D. Sherrington, AIP Conf. Proc. 29, 224 (1976). More recent theoretical papers are, e.g., D. A. Smith, J. Phys. B 4, L266 (1974); B. W. Southern, J. Phys. C 9, 4011 (1976);

D. J. Thouless, P. W. Anderson, E. Lieb, and R. G. Palmer, Princeton University report, 1976 (unpublished); J. M. Kosterlitz, D. J. Thouless, and R. C. Jones, Phys. Rev. Lett. 36, 1217 (1976); T. Plefka, J. Phys. F 6, L327 (1976).

[10]Nonsaturation of $M(H, T)$ up to 670 kG K^{-1} (Ref. 6) in Cu–186-ppm Mn is attributed by the authors to cluster effects.

[11]A. I. Larkin and D. E. Khmel'nitskii, Sov. Phys.-JETP 31, 958 (1970).

[12]A. I. Larkin, V. I. Mel'nikov, and D. E. Khmel'nitskii, Sov. Phvs.-JETP 33, 458 (1971).

[13]M. W. Klein, Phys. Rev. 173, 552 (1968); 188, 933 (1969).

[14]M. A. Ruderman and C. Kittel, Phys. Rev. 96, 99 (1954); T. Kasuya, Prog. Theor. Phys. 16, 45 (1956).

[15]K. Yosida, Phys. Rev. 106, 893 (1957).

[16]E. C. Hirschkoff, O. G. Symko, and J. C. Wheatley, J. Low Temp. Phys. 5, 155 (1971).

[17]A. Blandin, thesis (Paris University, 1961) (unpublished).

[18]J. Souletie and R. Tournier, J. Low Temp. Phys. 1, 95 (1969).

[19]W. Marshall, Phys. Rev. 118, 1519 (1960); M. W. Klein and R. Brout, Phys. Rev. 132, 2412 (1963).

[20]For a review, see M. D. Daybell, in *Magnetism V*, edited by H. Suhl (Academic, New York, 1973), p. 121.

[21]For a review see C. Rizzuto, Rep. Prog. Phys. 37, 147 (1974).

[22]J. R. Schrieffer and P. A. Wolff, Phys. Rev. 149, 491 (1966).

[23]P. W. Anderson, Phys. Rev. 124, 41 (1961); J. Kondo, Prog. Theor. Phys. 28, 846 (1962).

[24]For recent discussions, see the articles by D. K. Wohlleben and B. R. Coles, and by A. Narath in *Magnetism V*, edited by H. Suhl (Academic, New York, 1973).

[25]For a review see G. H. Nieuwenhuys, Adv. Phys. 24, 515 (1975).

[26]W. M. Star, S. Foner, E. J. McNiff, Jr., Phys. Rev. B 12, 2690 (1975).

[27]G. Williams, G. A. Swallow, A. D. C. Grassie, and J. W. Loram, AIP Conf. Proc. 24, 447 (1975).

[28]A. Amamou, R. Caudron, P. Costa, J. M. Friedt, F. Gautier, and B. Loegel, J. Phys. F 6, 2371 (1976)

[29]A preliminary report has appeared: H. C. Jones, A. G. Montogomery, I. B. Lin, J. W. Lue, H. Nadler, and R. R. Hake, Bull. Am. Phys. Soc. 22, 309 (1977).

[30]M. T. Béal-Monod and R. A. Weiner, Phys. Rev. 170, 552 (1968).

[31]R. A. Weiner and M. T. Béal-Monod, Phys. Rev. B 3, 145 (1971).

[32]H. C. Jones, A. G. Montgomery, I. B. Lin, J. W. Lue, H. Nadler, and R. R. Hake (unpublished).

[33]R. P. Elliott, *Constitution of Binary Alloys*, 1st Suppl. (McGraw-Hill, New York, 1965), p. 620.

[34]For reviews of Zr metallurgy see, e.g., B. Lustman and F. Kerze, Jr., *The Metallurgy of Zirconium* (McGraw-Hill, New York, 1965); G. L. Miller, *Zirconium* (Butterworths, London, 1954).

[35]R. R. Hake, D. H. Leslie, and T. G. Berlincourt, Phys. Rev. 127, 170 (1962).

[36]J. A. Cape, Phys. Rev. 132, 1486 (1963).

[37]R. R. Hake and J. A. Cape, Phys. Rev. 135, A1151(1964).

[38]Pacific Spectrographic Laboratory, Los Angeles, Calif.

[39]A. M. Clogston, B. T. Matthias, M. Peter, H. J. Williams, E. Corenzwit, and R. C. Sherwood, Phys. Rev. 125, 541 (1962).

[40]J. A. Cape and R. R. Hake, Phys. Rev. A 139, 142 (1965).

[41]Dr. E. Parry, (private communication).

[42]E. C. Stoner, Philos. Mag. 36, 803 (1945).

[43]The average cross-sectional area $\langle A\rangle$ over the central 1.0-cm zone sensed by both the resistive potential leads and the magnetometer search coils was estimated by assuming $\langle A\rangle = \frac{1}{4}\pi\langle d\rangle^2$ where $\langle d\rangle = (\frac{1}{4})(d_r + 2d_0 + d_l)$. Here the subscripts refer to the right edge, center, and left edge, respectively, of the central zone, and $d = d_{\min} + d_{\max}$ as located and read with a 0.016-in.-thick-blade micrometer. The smooth axial and radial variations in d, which resulted primarily from the etching, were less than ± 3% and ± 1%, respectively. We estimate the accuracy of $\langle d\rangle$ and $\langle A\rangle$ to be ± 1.5% and ± 3%, respectively. Since $\rho \propto A/l$, where l is the potential lead spacing (uncertain to ± 2%), the total geometry-related uncertainty in ρ is ± 5%. Since for M the calibration procedure results in errors $\propto A^{-1}$, geometry-related uncertainty in M is ± 3%.

[44]See Ref. 35 and references cited therein.

[45]E. D. Ramos, J. Low Temp. Phys. 20, 547 (1975).

[46]R. R. Hake, Phys. Rev. 158, 356 (1967).

[47]J. W. Lue, A. G. Montgomery, and R. R. Hake, Phys. Rev. B 11, 3393 (1975).

[48]A. G. Montgomery, Ph.D. thesis (Indiana University, 1976) (unpublished).

[49]R. J. Harrison and M. W. Klein, Phys. Rev. 154, 540 (1967); M. W. Klein, *ibid.* 173, 553 (1968).

[50]J. L. Tholence and R. Tournier, J. Phys. (Paris) 35, C4-229 (1974).

[51]J. W. Loram, T. E. Whall, and P. J. Ford, Phys. Rev. B 3, 953 (1971).

[52]P. Monod, Phys. Rev. Lett. 19, 1113 (1967).

[53]A. E. Bell and A. D. Caplin, J. Phys. F 5, 143 (1975).

[54]See, e.g., Eq. (2.2) of Ref. 20. We refer to this as the Hamann-Fischer formula.

[55]B. Caroli, J. Phys. F 5, 1399 (1975).

[56]For a discussion of the exchange parameter J as determined by various types of measurements, see Ref. 55; D. Davidov, K. Maki, R. Orbach, C. Rettori, and E. P. Chock, Solid State Commun. 12, 621 (1973); R. E. Walstedt and L. R. Walker, Phys. Rev. B 11, 3280 (1975); Ref. 57.

[57]D. Davidov, C. Rettori, R. Orbach, A. Dixon, and E. P. Chock, Phys. Rev. B 11, 3546 (1975).

[58]For comparison, the formula (from Ref. 20 but with misprints corrected) for the unitary limit for d-wave scattering $\rho_{du} = 10\, m^* c_f V_m/\pi Z e^2 N_b(0)\hbar N_a$ [where m^* is the effective electron mass, V_m is the molar volume, Z is the number of conduction electrons per host atom, $N_b(0)$ is the bare single-spin density of states per atom, and N_a is Avogardro's number] yields 1.2 nΩ cm/ppm for Zr (using the Zr parameters of Ref. 59) as compared to 1.9 nΩ cm/ppm for Cu. The total step heights $[\Delta\rho(T=0) - \Delta\rho(T=\infty)]/c = (\rho_{du}/c)\cos 2\delta_v$ of the resistivity as predicted by the present fits are: 0.90, 0.57, 0.39, 0.32 nΩ cm/ppm for, respectively, $T_K = 0.001$, 0.01, 0.1, 1.0 K.

[59]The molar volume V_m for Zr at 4.2 K is taken as 13.88 cm^3/mole from K. A. Geschneidner, Solid State Physics 16, 275 (1964) [a 1% correction was applied to the tabulated V_m ($\approx$300 K) = 14.02 cm^3/mole for volume contraction between 300 and 4.2 K]. The assumption that all electrons outside closed shells in Zr are con-

duction electrons implies $Z=4$, and hence a conduction-electron concentration $N=ZN_a V_m^{-1}=1.74\times10^{23}$ cm^{-3}. Assuming a free-electron model: $k_F=(3\pi^2N)^{1/3}=1.73\times10^8$ cm^{-1}, $V_f=\hbar k_F/m_e=2.00\times10^8$ cm sec^{-1}, $\epsilon_F=(\frac{1}{2})mV_F^2=11.4$ eV, $N_b(0)=3Z/4\epsilon_F=0.26$ (single spin states)/(eV atom), $\gamma_0=N(0)/0.212=1.24$ mJ/mole K^2. The thermal effective mass ratio is then $(m^*/m_e)_{th}=\gamma$ (measured)$/\gamma_0=2.80/1.24=2.25$ using the γ measured by E. D. Kneip, J. O. Betterton, and J. O. Scarbrough, Phys. Rev. 130, 1687 (1963).

[60]The $\epsilon_F=8.2$ eV value is indicated by band-structure calculations of T. L. Loucks, Phys. Rev. 159, 544 (1967); see also K. Iyakutti, C. K. Majumdar, R. S. Rao, and V. Quenneville, J. Phys. F 6, 1636 (1976).

[61]For recent recommendations on units in magnetism see L. H. Bennett, C. H. Page, and L. J. Swartzendruber, AIP Conf. Proc. 29, preface (1976).

[62]N. V. Volkenshteyn and E. V. Galoshina, Fiz. Met. Metalloved 20, 368 (1965).

[63]C. F. Squire and A. R. Kaufmann, J. Chem. Phys. 9, 673 (1941). [We linearly extrapolate their data at $T\geq50$ K so as to ignore an apparent magnetic-impurity-induced negative slope in $\chi(T)$.]

[64]N. V. Volkenshteyn, E. V. Galoshina, and N. I. Shchegolikhina, Fiz. Met. Metalloved 25, 180 (1968). See also E. W. Collings and J. C. Ho, Phys. Rev. B 4, 349 (1971).

[65]R. B. Frankel, N. A. Blum, B. B. Schwartz, and D. J. Kim, Phys. Rev. Lett. 18, 1051 (1967).

[66]J. W. Loram, A. D. C. Grassie, and G. A. Swallow, Phys. Rev. B 2, 2760 (1970); G. A. Swallow and R. J. White, Solid State Commun. 10, 361 (1972).

[67]R. W. Schmitt and I. S. Jacobs, J. Phys. Chem. Solids 3, 324 (1957); I. S. Jacobs and R. W. Schmitt, Phys. Rev. 113, 459 (1959).

[68]M. D. Daybell and W. A. Steyert, Phys. Rev. Lett. 20, 195 (1968).

[69]R. Berman and J. Kopp, J. Phys. F 3, 847 (1973).

[70]E. W. Fenton, Phys. Rev. B 7, 3144 (1973); 5, 3788 (1972).

[71]For a review of early data, most of it representing the moment-moment interaction regime, see G. J. Van den Berg, in *Progress in Low Temperature Physics* (North-Holland, Amsterdam, 1964), Vol. IV, p. 194.

[72]P. L. Li and B. E. Paton, Phys. Lett. A 56, 225 (1976).

[73]H. Rohrer, Phys. Rev. 174, 583 (1968).

[74]C. M. Hurd and J. E. A. Alderson, Phys. Rev. B 6, 1894 (1972).

[75]F. T. Hedgcock, W. B. Muir, T. W. Raudorf, and R. Szmidt, Phys. Rev. Lett. 20, 457 (1968).

[76]R. W. Cochrane, F. T. Hedgcock, A. W. Lightstone, and J. O. Ström-Olsen, AIP Conf. Proc. 24, 71 (1975).

[77]F. T. Hedgcock, J. O. Ström-Olsen, and D. Wilford, *Proceedings of the Fourteenth International Conference on Low Temperature Physics*, edited by M. Krusius and M. Vuorio (North-Holland, 1975), Vol. 3, p. 298.

[78]R. W. Cochrane, F. T. Hedgcock, and J. O. Ström-Olsen, Phys. Rev. B 8, 4262 (1973).

[79]The 2 in front of $(2S+1)$ is as specified in an erratum to Ref. 11 which appears in Ref. 12 under Eq. (38).

[80]M. W. Klein, Phys. Rev. B 14, 5008 (1976); B. Fischer and M. W. Klein, 14, 5018 (1976); M. W. Klein (private communication).

[81]Reference 4 utilizes an expression similar to Eq. (27) but with the right-hand side multiplied by $\pi S(S+1)(2\sqrt{2})^{-1}$. Equation (27) is consistent with the V_0-J relationship utilized in Ref. 1. Following Eq. (3.12) of Ref. 15, Eq. (27) assumes that J_{RKKY} is independent of the wave vector.

[82]R. J. Harrison and M. W. Klein, Ref. 49.

[83]R. More and H. Suhl, Phys. Rev. Lett. 20, 500 (1968).

[84]Recent studies in the transition-metal–base Mo-Fe system (Ref. 28) show that, contrary to the usual behavior of non-transition-metal-host systems, peaks in the specific heat are not accompanied by peaks in the susceptibility.

[85]For comparison, Ref. 21, Table IIb lists $\Delta\rho/c=4.8\,\mu\Omega$ cm/at.% for Mn in Cu. Thus for carefully prepared Cu-Mn alloys one expects $\rho(4.2\text{ K})\approx0.24$, $1.5\,\mu\Omega$ cm at Mn concentrations of, respectively, $c=520$, 3100 ppm. These residual resistivities are factors of 10 and 3.5 smaller than the residual resistivities of the present corresponding Zr-Mn alloys.

[86]P. G. de Gennes, J. Phys. Radium 23, 630 (1962). O. Béthoux, J. A. Coreaga, B. Dreyfus, K. Gobrecht, J. Souletie, R. Tournier, J. J. Veyssié, and L. Weil, in Ref. 6, p. 290; J. L. Tholence and R. Tournier, J. Phys. (Paris) 32, C1-211 (1971).

[87]M. W. Klein, Phys. Lett. A 59, 52 (1976).

[88]I. Riess and M. W. Klein, Phys. Rev. B (to be published).

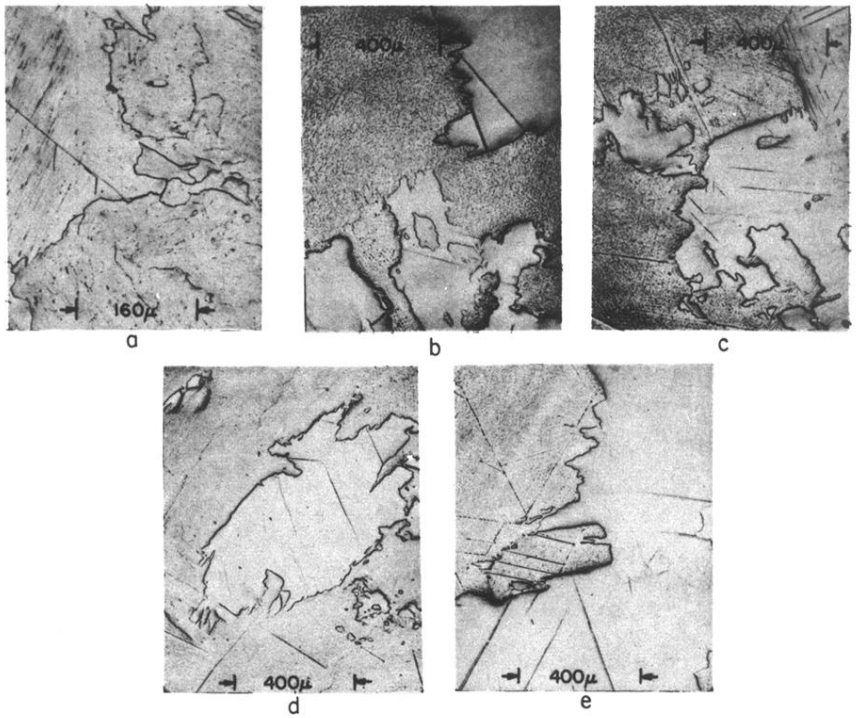

FIG. 1. Photomicrographs representative of (a) "pure" Zr specimen Zr No. 1, (b) Zr-520 ppm Mn, (c) Zr-900 ppm Mn, (d) Zr-1690 ppm Mn, (e) Zr-3100 ppm Mn.